

## Article

# Occurrence Characteristics of Magnetite and Aeromagnetic Prospecting Northeast of Hebei Province

Yan-Xu Liu <sup>1</sup>, Wen-Yong Li <sup>1,\*</sup>, Zhi-Yuan Liu <sup>2</sup>, Jia-Wei Zhao <sup>2</sup>, An-Qi Cao <sup>1</sup>, Shan Gao <sup>1</sup>, Li-Jie Wang <sup>3</sup> and Cheng Yang <sup>3</sup>

<sup>1</sup> China Aero Geophysical Survey and Remote Sensing Center for Nature Resources, Beijing 100083, China

<sup>2</sup> Hebei Institute of Geological Survey, Shijiazhuang 050081, China

<sup>3</sup> Oil and Gas Engineering Research Institute of Jilin Oilfield Company, Songyuan 138000, China

\* Correspondence: liwenyong@mail.cgs.gov.cn; Tel.: +86-010-6206-0153

**Abstract:** The occurrence characteristics of magnetite and the methods to quickly and effectively explore are important topics for ore prospecting in the new era. Taking northeast of Hebei Province of China as an example, this article aimed at an important strategic mineral of magnetite, then discussed its distribution characteristics and aeromagnetic exploration methods of it. First of all, we discuss the occurrence characteristics of sedimentary metamorphic and magmatic magnetite. Then, using the latest high-precision aeromagnetic data, combined with the geological outcrops, known iron deposits, ground magnetic surveys, and verification, we studied the relationship between the aeromagnetic anomalies and iron deposits through potential field conversion processing of the reduction to the pole, vertical derivative, upward continuation and residual anomaly, and the forward modeling and inversion methods of 2.5 D optimization fitting. Next, we summarize the metallogenic conditions and attributes of aeromagnetic prospecting and make magnetite predictions. In addition, it has suitable magnetite prospecting potential in the Laochenjia, Dabai, Jiuwuying, Beierying, Sidaogoumen, and Wuyingzi aeromagnetic anomaly regions. In conclusion, these regions have aeromagnetic anomalies with high amplitudes, large scales, and favorable metallogenic backgrounds for magmatic rocks, strata, and structures caused by concealed magnetite. In addition, they have great prospecting potential. Eventually, we hope this research method in this article can provide a reference for magnetite exploration in other areas with similar geological conditions.

**Keywords:** magnetite; occurrence characteristics; aeromagnetic anomaly; prospecting prediction; northeast Hebei



**Citation:** Liu, Y.-X.; Li, W.-Y.; Liu, Z.-Y.; Zhao, J.-W.; Cao, A.-Q.; Gao, S.; Wang, L.-J.; Yang, C. Occurrence Characteristics of Magnetite and Aeromagnetic Prospecting Northeast of Hebei Province. *Minerals* **2022**, *12*, 1158. <https://doi.org/10.3390/min12091158>

Academic Editor: Stanisław Mazur

Received: 2 August 2022

Accepted: 7 September 2022

Published: 14 September 2022

**Publisher's Note:** MDPI stays neutral with regard to jurisdictional claims in published maps and institutional affiliations.



**Copyright:** © 2022 by the authors. Licensee MDPI, Basel, Switzerland. This article is an open access article distributed under the terms and conditions of the Creative Commons Attribution (CC BY) license (<https://creativecommons.org/licenses/by/4.0/>).

## 1. Introduction

The metamorphic supracrustal rocks and metamorphic plutonic rocks of the early Precambrian are widely distributed in the study region. Regional folds and fault structures are well developed [1,2]. There are many magmatic intrusion periods. Propitious regional geological and metallogenic conditions provide abundant material sources, heat sources, and storage spaces for the formation of iron ore resources [3,4].

The mineralization mainly includes two types in the study region metamorphic mineralization and magmatic mineralization [5–12]. Metamorphic mineralization refers to the change in formed rocks and deposits under specific physical, chemical, or geological conditions. This leads to the migration and enrichment of the rearrangement and redistribution of ore-forming materials. It includes regional metamorphism, contact metamorphism, and dynamic metamorphism. Among them, regional metamorphism is one of the most typical and important types of metamorphic mineralization in the study region. Magmatic mineralization refers to differentiation and crystallization leading to the accumulation of useful materials dispersed in magma during the generation, migration, or emplacement of various magmas. Alternatively, in special cases, it is a process in which useful materials

dispersed in magma consolidate into a geological body with economic value. Because of the complex composition of the magma, it is generally composed of silicate, heavy metals, and some volatile components. During the condensation process, magmatic crystallization differentiation often occurs. This kind of action can enrich some useful materials and form deposits. It is termed mineralization of magmatic differentiation and magmatic crystallization. Magmatic differentiation and crystalline deposits have developed to a certain extent in this region. The typical representative is a magnetite type of magmatic rock (vanadium titanium) [9,11–19].

At present, known deposits of sedimentary magnetite and magmatic magnetite have indications of high-amplitude aeromagnetic anomalies [20–23]. After we used aeromagnetic and potential field data in defining potential mineral exploration targets and gold deposit prospective regions, they can reveal the suitable prospects of iron and polymetallic ore [24–29]. After aeromagnetic surveying and ground investigation of key anomalies, a significant number of large and medium-sized iron ore deposits have been found in the abnormal area of unknown ore occurrences. Over the past 40 years, Hebei Province of China has made substantial achievements in searching for magnetic minerals (by direct methods) and polymetallic minerals (by indirect methods) using the aeromagnetic measurement characteristics of high resolution, accurate positioning, and high reliability [23,30–36].

In recent years, magnetite deposits in the surface and shallow regions in Hebei Province have been identified. This means that the difficulty of further prospecting has increased significantly. At present, most of the aeromagnetic data used in magnetite prediction and research belong to the first generation of aeromagnetic maps. Compared with the existing high-precision aeromagnetic data, the previous aeromagnetic data have the following: the magnetic field level was not unified in different survey intervals; the scale and contour spacing were inconsistent; the positioning level and observation accuracy were low; the low and gentle anomalies (especially the weak anomalies) were difficult to find; these low and gentle anomalies often reflect deep ore bodies [37–39]. If the accuracy and quality of data are low, it will be difficult to meet the exploratory task of ore prospecting breakthroughs and achieve major breakthroughs in geological prospecting [40,41].

Therefore, limited by the scale and accuracy of previous surveys, many anomalies with prospecting potential have not been discovered or systematically studied [40,41]. These are one of the key directions for the next exploration breakthrough. Using the latest high-precision aeromagnetic survey data covering northeastern Hebei Province, we aim to study the typical aeromagnetic anomaly characteristics of sedimentary iron ore and magmatic rock iron ore and then predict iron ore prospecting on the basis of summarizing geological and aeromagnetic prospecting indicators to provide important geophysical information for magnetite prospecting breakthroughs.

## 2. Geological Background

### 2.1. Stratum

The study region belongs to the stratigraphic region of North China. It crosses the stratigraphic region of Yinshan-northern Hebei and Yanliao. The crystalline basement was formed at the end of the Palaeoproterozoic. It is overlain by the sedimentary cover. The difference from the typical platform region is the strong activity transformation in the Mesozoic and Cenozoic.

The strata in the study area developed from bottom to top, including Neoproterozoic, Proterozoic, Lower Paleozoic, Upper Paleozoic (sporadically exposed), Mesozoic, and Cenozoic strata [42–45]. The Neoproterozoic is mainly distributed in the southern part of the study region. It is a set of medium–deep metamorphic rock series. The Paleoproterozoic is mainly distributed north of the Shangyi-Longhua regional fault, which is a set of shallow–medium metamorphic rock series. The meso-neo-Proterozoic is the first set of stable caprocks above the metamorphic basement of the North China Craton. It is mainly composed of stable marine magnesium-rich carbonate rocks that are not metamorphosed or lightly metamorphosed. There are abundant iron, manganese, pyrite, lead, zinc, and other

nonmetallic minerals in the meso-neo-Proterozoic. The Paleozoic is not well developed in the region. Only the Cambrian and Permian are developed. The exposed region is only in the northeast of Weichang. The Mesozoic is widely exposed in the region. It is a set of volcanic-sedimentary rock series and is mainly composed of continental clastic rocks and intermediate-acidic volcanic rocks interbedded with coal seams and oil shale. The Cenozoic is widely distributed north of Weichang and mostly belongs to continental sediments and basic volcanic rock accumulation.

## 2.2. Structure

With the exploration of regional geological structures and the revelation of deep structures, tectonic evolution played an important role in the analysis of crustal structure and the development of geological structures [46,47].

The study region is in the northeastern North China Craton of the Chaidamu-North China plate. It involves three tectonic units as follows: the subsidence (active) zone in the northern margin of North China, the uplift zone in the northern margin, and the rift zone of Yanshan-western Liaoning. The faults and fold structures are well developed under the control and influence of multiperiod tectonic movements. The structures have different strike directions, mainly including the near-EW, -NE, and -NW directions. Multiple groups of structures intersect, cut, compound, or superimpose each other [43–45,48–51]. They form the complex structural features of the study region.

The regional fault structures are mainly the Kangbao-Weichang fault, Shangyi-Chicheng-Longhua fault, and Shanghuangqi-Wulonggou fault. The Kangbao-Weichang fault is located from south of Kangbao to north of Weichang. It has a nearly E–W-trending serpentine shape. It was formed in the Late Neoproterozoic. It had the characteristics of long-term activity, multiperiod activity, variable tendency, and variable nature. This activity was strongest at the end of the Permian and was accompanied by a large amount of magmatic rock intrusion. This fault was still active in the Mesozoic. The Shangyi-Chicheng fault was also formed in Late Neoproterozoic, with a nearly E–W-trending distribution and, in addition, was highly deformed. The northern section of the Shanghuangqi-Wulonggou fault (N-NE direction) breaks through the northwest corner of the study region. This fracture has a strong and complex deformation. The fault and the magmatic rocks that are controlled by it form a tectonomagmatic rock belt of large-scale and N-NE trends.

## 2.3. Intrusive Rock

According to the differences of formation environment, heterogeneity of fault activity, and different formation times, the size of magmatic rocks is quite different and the lithofacies and rock types are diverse. It even presents the landscape of magmatic rock belt with specific spatial distribution rules. Magmatic activities often have important influences on regional tectonic history [52,53].

Intrusive rocks are well developed in both the study region and its adjacent regions. These spread throughout the entire region in spatial distribution. Magmatic activity is very frequent in the study area and its periphery and can be divided into six magmatic cycles as follows: Neoproterozoic, Paleoproterozoic, Mesoproterozoic, Late Paleozoic, Mesozoic, and Cenozoic (from old to new) [49–51]. Among them, Hercynian and Yanshanian magmatic activities are the most intense (Figure 1) and have the largest exposed regions. Magmatic intrusion in the late Jurassic–Early Cretaceous was very frequent. The magmatic intrusion of the Late Paleozoic takes second place. Intrusive rocks of the Neoproterozoic have been deeply metamorphosed into gneisses, while intrusive rocks of the paleo-Proterozoic have been metamorphosed into metamorphic plutonic rocks.

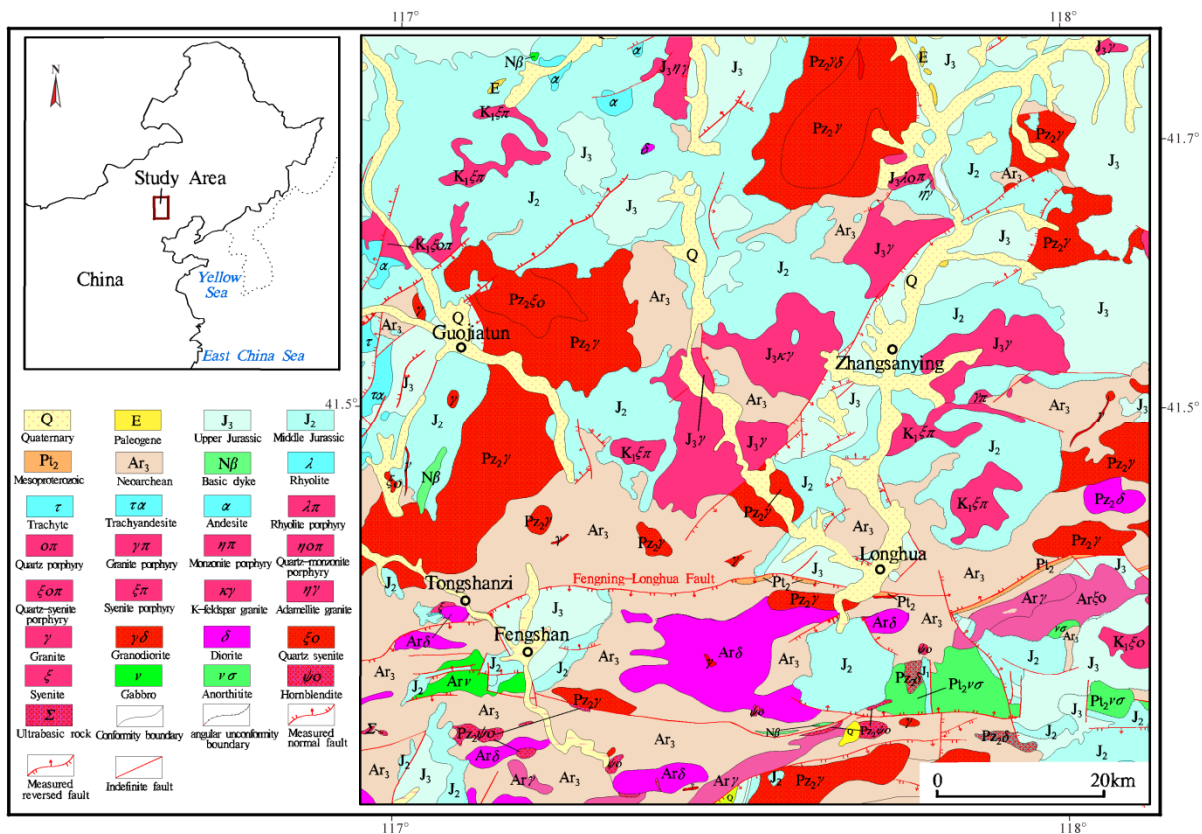


Figure 1. Geological map of the study region.

### 3. Occurrence Characteristics of Magnetite in the Study Region

#### 3.1. Sedimentary Metamorphic Magnetite

Metamorphic iron deposits (iron deposits of regional metamorphic) are mainly distributed in the southern part of the study region. In the process of plate movement, due to the large-scale tectonic stress accompanied by different degrees of flow anomalies from tectonic heat and upwelling from deep magma, under the combined action of high temperature, high pressure, and magmatism, sedimentary iron deposits or sedimentary iron-bearing formations (Dantazi Group et al.) underwent regional metamorphism or migmatization after forming in the Neoproterozoic. Following this, the regional metamorphic iron ore formed through large-scale strong reorganization and transformation. Thus, it can also be called regional metamorphic iron deposits.

The mineralization of regional metamorphic iron deposits in this region has the following characteristics: (1) The formation is closely related to rift volcanic activity in active continental margins both in time and space. It developed in the new Archean greenstone belt (Dantazi Group et al.). It is mainly associated with pyroclastic facies in the middle and upper parts of the greenstone belt and is close to the turbidite assemblage. The original rocks are basic volcanic rocks with a few andesitic rocks, intermediate-acid volcanic rocks, and clayey sedimentary rocks. Generally, it has undergone regional metamorphism of greenschist facies and amphibolite facies. The original basic volcanic rocks metamorphosed into amphibolite, amphibolite schist, amphibolite plagiogneiss, granulite, granulite, among others. The original intermediate-acid volcanic rocks metamorphosed into biotite granulite, hypabyssal granulite, etc. (2) The Neoproterozoic iron deposits have been transformed by regional metamorphism to different degrees. Most of this transformation is carried out in a basically closed system. Under the condition that the total chemical composition of the original ore bed remains unchanged, the result of transformation is the recrystallization of minerals, the recombination of mineral phases, and the deformation and relocation of ore bodies. The mineral composition of the oxide phase in ferrosilicon formation is relatively

simple. Under any degree of metamorphism, the composition of iron ore is basically unchanged, and is mainly composed of magnetite, haematite, and quartz. To varying degrees, the development of recrystallization can increase the mineral particles. However, further enrichment of iron ore is not significant. If the metamorphism further develops to the migmatization stage, not only the oxide phase but also the mineral composition with silicate phase (including iron) will also become significantly transformed. The ferrosilicon formation can be replaced by a combination of amphibole, magnetite, and quartz. Even granulite is accompanied by assemblages of pyroxene, diopside, magnetite, quartz, etc. At the same time, migmatized fluid can further enrich iron to form iron-rich ore. (3) The shape of this kind of iron ore is usually a narrow-banded structure composed of gray or light dark green iron chert, haematite, or magnetite. The thickness of a single ore body can range from just a few to hundreds of meters. The strike extends can range from meters to several kilometers. A series of continuous and convex mirror-shaped ore bodies in ore-bearing formations form a large-scale ore belt. (4) The important deposit type in this region is sedimentary metamorphic iron deposits of the Anshan type. It is mainly distributed in the metamorphic supracrustal rocks in the early Precambrian in the southern survey area. The position of iron deposits is mainly in the Dantazi group. A high number of Neoproterozoic metamorphic rock series are developed in the south of the region. This type of metamorphic iron deposit has a vast distribution area and large reserves.

### 3.2. Magmatic Magnetite

Although the number of known deposits is limited, the type of magmatic magnetite has distinct metallogenic characteristics, strong regularity, and great prospecting potential. The main features are as follows: (1) The magnetite (vanadium titanium) occurs in basic rocks (anorthosite, norite, and gabbro) in the process of differentiation and crystallization of magma (containing vanadium, titanium, and iron), and rock-forming minerals crystallize. Then, ore-forming materials of vanadium, titanium, and iron accumulated in the residual magma. When the magma was about to consolidate, vanadium, titanium, and iron minerals crystallized intensively to form magnetite. (2) Magnetite (vanadium titanium) ore bodies are distributed along certain fractures in basic rocks or the contact zone of norite, gabbro, and anorthosite. (3) The boundaries of basic rocks containing magnetite (vanadium titanium) are mostly fault structures. This shows that the fault structures have obviously controlled the ore-bearing rocks. (4) Magmatic magnetite of the Damiao type is related to the mafic and ultrabasic intrusive rocks in the Mesoproterozoic and late Palaeozoic. The magnetites were controlled by deep and large faults. Basic and ultrabasic rocks are mainly distributed along the regional fault zone from Shangyi to Longhua and the adjacent regions. More than 100 basic and ultrabasic rock bodies have been found. Iron ore deposits mostly exist in Chongli-Chengde basic and ultrabasic rocks. This type of rock has a large scale and is well differentiated with rich and large magnetites (vanadium titanium). For example, the anorthosite and norite bodies in the Damiao-Tougou region of Chengde are typical large-scale bodies in China [9,14,35,49]. They are rich in magnetite (vanadium titanium). (5) There are many aeromagnetic anomalies with similar characteristics to basic and ultrabasic intrusive rocks of the known ore bearing (magnetite). It is inferred that they were caused by basic and ultrabasic intrusive rocks are a favorable target in searching for the magnetite type of magmatic rock (vanadium titanium). It has great prospecting potential.

## 4. Data

### 4.1. Data from Aeromagnetic Survey

The aeromagnetic survey was carried out with the HC-2000 helium optically pumped magnetometer system (developed by AGRS, i.e., China Aero Geophysical Survey and Remote Sensing Center for Land and Resources, Beijing, China), with a sensitivity of 0.005 nT and a sampling rate of 10 times per second. The survey scale is 1:25,000, with the interval of adjacent survey lines of 250 m and survey line direction of 0–180°. The interval of the adjacent cross line is 5 km, and the cross-line direction is 90–270°. The flight

height is 120–350 m from the ground. The total accuracy of the aeromagnetic survey after leveling and noise processing (the mean square deviation of aeromagnetic differences for intersection points between survey lines and cross lines) is 1.79 nT.

The processing of aeromagnetic data includes two steps: field preprocessing and indoor processing. The field preprocessing includes data input, assessment of acquisition quality control, statistics of parameters, correction of aeromagnetic data, coordinate transformation, drawing of flying routes, flying heights, and aeromagnetic profiles. The indoor processing includes merging of flight database, data checking and editing, coordinate transformation, correction of aeromagnetic normal field, correction of magnetic diurnal variation, lag correction, aeromagnetic leveling, statistics of survey quality control, and basic graphics drawing. The data processing was carried out with the Geoprobe Mager software (developed by AGRS, Beijing, China), the Oasis Montaj software (developed by Geosoft Inc., Toronto, ON, Canada), the AgsMGis software (developed by AGRS, Beijing, China) and the MapGis software (developed by Wuhan Zhongdi Digital Technology Co., Ltd., Wuhan, China). After processing and interpolation, we obtained the aeromagnetic data with a grid of 50 m  $\times$  50 m using the gridding method of Kriging (Figure 2).

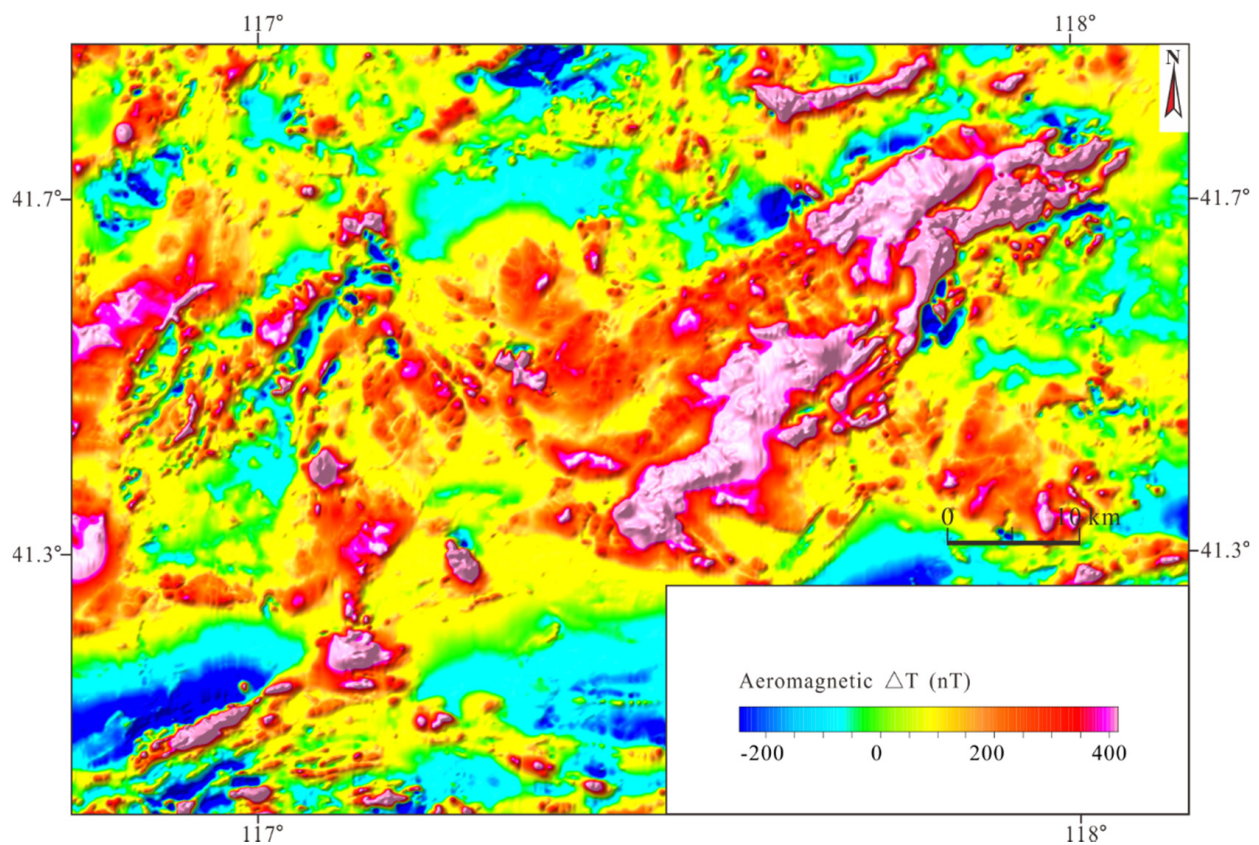


**Figure 2.** Aeromagnetic  $\Delta T$  of the study region.

#### 4.2. Data from Ground Survey

The ground magnetic survey was carried out with an HC95 optical pumping magnetometer DWJ-1 (developed by AGRS, Beijing, China). The measurement parameter is total magnetic field  $T$ . The total accuracy of magnetic measurement is  $\pm 5$  nT. The anomaly area is evaluated by the average relative error, which should not be more than 5%.

We obtained the data of the electric method using DC induced polarization. The device (developed by IGGE, Beijing, China) of electrode array includes intermediate gradient and symmetric quadrupole sounding arrangement. The point distance is 10 to 20 m. The quality inspection rate of the IP intermediate gradient device is 11.60%. The mean square error of apparent resistivity and polarization rate is 6.54% and 4.89%. IP intermediate gradient

profile was arranged with a spacing of 50 m and a point distance of 20 m. A total of 8 fixed-point source sounding and 20 controlled source audio-frequency magnetotellurics points were arranged on the profile. The distance between fixed-point source sounding points is 40, 60, and 80 m. The distance between controlled source audio-frequency magnetotellurics points is 40 m.

The soil geochemistry profiles were produced on the main profile, which is the same as ground magnetic and electrical profile. The sampling points are consistent with the points of ground magnetic profile. A total of 11 elements from the samples were analyzed including Au, Ag, As, Sb, Cu, Pb, Zn, W, Mo, Bi, and Sn. Detection limit, accuracy, precision, and reporting were obtained from the analysis data of these samples. The qualification rate of the samples of the 11 main ore-forming elements is more than 90%.

#### 4.3. Potential Field Conversion

Potential field conversion is the basic method of aeromagnetic interpretation. In view of the specific target of this aeromagnetic interpretation, we adopted the processing of potential field conversions such as the reduction to the pole, vertical derivative, upward continuation, and residual anomaly with the Geoprobe Mager software.

#### 4.4. Forward and Optimization

The essence of forward modeling and optimization is to recognize the geological bodies causing the field anomaly by modifying the geological model and parameters and making the theoretical field data conform to the measured field data. Based on the measured field data and combining the physical properties of rocks or ores, we produce the geological model with the best fit between the theoretical and measured curve, and the model parameters generating the best-fit curve are the result.

The specific steps are as follows: (1) The measured anomaly values and coordinates are input. (2) The geological models are selected. The model selection is based on the characteristics of magnetic anomalies and the known geological environment in the study area. (3) The parameters of the geomagnetic field and model are given. First, the parameters of geomagnetic field are given, with the geomagnetic inclination of  $60.5^\circ$  and the geomagnetic declination of  $-7.3^\circ$ . Second, the model parameters are given, such as vector directions of remanence, magnitude of magnetic susceptibility, and magnitude of remanence, which are dependent on the actual measurement data from strata, rocks and ores in the study area. (4) The theoretical anomaly for the geological model is computed and compared with the measured anomaly. (5) The fitting degree between the theoretical and measured curves is evaluated, and whether or not the geological model will be modified and the theoretical curve will be recomputed. (6) If the difference between the theoretical and measured curves does not meet the requirement, the model will be modified until the requirement is satisfied. (7) The model parameters are output as the forward result. The above process is conducted by computer using visualization software.

We used the Euler deconvolution method to invert the depth of magnetic body in the study region (Figure 3), then extracted the fractures information from the magnetic data using this edge method. By using the field values of aeromagnetic data  $\Delta T$ , the gradient values of aeromagnetic data  $\Delta T$ , and the linear equations describing the system, we can solve the unknown variables of depths of magnetic body. Then, the structural trace can be determined.

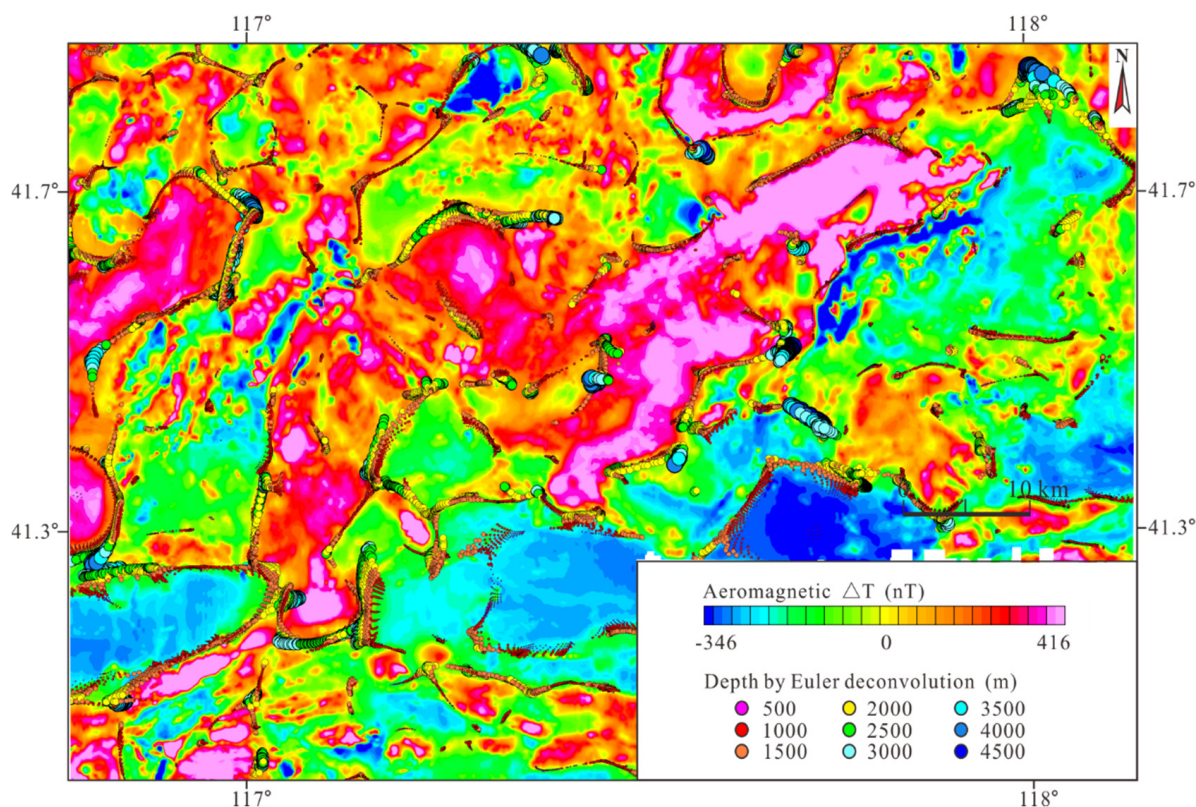


**Figure 3.** Reduction to the pole of aeromagnetic  $\Delta T$  and depth by Euler deconvolution of the study region.

## 5. Aeromagnetic Response of Magnetite and Nonmagnetite

### 5.1. Magnetic Characteristics

Using field measurement data (including 17,687 magnetic susceptibility data, 68 magnetic orientation specimens, and 68 groups of remanence data), we obtained relevant statistics and analyzed the magnetic susceptibility parameters of the study. There are significant differences in the magnetism of sedimentary rocks, metamorphic rocks, magmatic rocks, and magnetite in the study region (Table 1).

In general, the magnetism of metamorphic rocks and magmatic rocks is strong. The sedimentary rocks are weak. The magnetic susceptibilities of the same type of rocks are obviously different because of the different lithologies. The sedimentary rocks mainly include silty sand, sandy soil, glutenite, limestone, and dolomite. They all have weak or very weak magnetism. They cannot cause obvious positive magnetic anomalies. The magnetism of sedimentary rocks from the Meso Neoproterozoic to Cenozoic is not strong because the magnetism of rock-forming minerals (mainly quartz, feldspar, carbonate, etc.) was very low. Most of them are diamagnetic. Therefore, normal sedimentary rocks are basically a set of strata without magnetism, making it impossible to cause a positive magnetic anomaly.

It can be summarized into two main magnetic layers in this region. One layer is the metamorphic rock series that makes up the crystalline basement. It includes the Neoproterozoic and Paleoproterozoic. Due to the differences in metamorphic degree, the layer has different magnetism, which can cause different degrees of magnetic anomalies. Another layer is the pyroclastic rock series of the Jurassic and Cretaceous and includes volcanic (clastic) rock and sedimentary clastic rock. Due to their different lithologies, compositions, and ferromagnetic mineral contents, they show different magneticities. This often causes obvious positive magnetic anomalies with a marked jump. Intrusive rocks are magnetic to varying degrees. Among them, ultrabasic and basic rocks have the strongest magnetism. If it has a certain scale, it can cause a strong magnetic anomaly. Most intermediate-acid and acid

rocks have certain magnetism, which can cause local magnetic anomalies. Magnetite is the geological body with the highest magnetism. It will cause an obvious high-amplitude positive magnetic anomaly if it has a certain scale. Magnetite or magnetite quartzite has extremely strong magnetism in the study region. Physical property data show that the average magnetic susceptibility can reach  $41,293 \times 10^{-5}$  SI. The maximum magnetic susceptibility is  $210,000 \times 10^{-5}$  SI. It also has a large remanence and vast magnetic differences from the surrounding rocks. Therefore, magnetite or magnetite quartzite with a certain scale can cause obvious high-amplitude positive magnetic anomalies. Such anomalies are easy to identify and provide the most intuitive basis for searching for magnetite or magnetite quartzite. Except for the strong magnetism of magnetite or magnetite quartzite, due to the influence of mineralization, the magnetism of some surrounding rocks containing magnetite is also significantly enhanced.

**Table 1.** Magnetic statistics of measured rock (ore) in the study region.

Lithology Classification	Lithology	Measured Points	K ( $\times 10^{-5}$ SI)		
			Minimum Value – Maximum Value	Arithmetic Mean Value	
Sedimentary rock	Silty sand, Sandy soil, Glutenite, Sandstone, Mudstone	1322	3–173	52	
	Limestone, Dolomite	275	1–64	9	
Metamorphic rock	Amphibolite, Gneiss granulite, Meta granulite, Shallow granulite, Migmatite, Magnetite amphibole	2522	3–18,315	1325	
	Quartz schist, Slate, Metamorphic sandstone	751	3–405	62	
	Marble, Quartzite	452	0–143	11	
Volcanic rock	Acidic rock	Rhyolite, Rhyolitic tuff, Rhyolitic volcanic breccia	1474	5–1294	263
	Intermediate rock	Trachyte	270	23–3411	385
		Trachyandesite	602	3–2632	1109
		Andesite, Andesitic tuff, Andesitic volcanic lava	1988	11–10,560	1183
	Basic rock	Basalt	784	159–7504	1209
Intrusive rock	Acidic rock	Granite porphyry	361	9–1315	227
		Granite	1267	25–8463	862
	Intermediate-acid rock	Granodiorite porphyrite	180	742–1956	962
		Granodiorite	330	20–3901	1026
	Basic rock	Syenite porphyry	961	15–3602	302
		Monzonite	963	11–8297	534
		Syenite	842	4–1578	591
		Diorite porphyrite	120	941–4569	1429
		Diorite	420	14–6155	1858
		Diabase	150	38–4986	1072
Ultrabasic to basic rock	Gabbro	120	441–5834	2117	
	Pyroxenite	150	1091–12,647	2472	
Mineral	Magnetite or magnetite quartzite	933	912–210,000	41,293	
	Hematite	120	42–327	102	
	Polymetallic minerals (lead, zinc, and silver)	120	6–19	13	
	Auriferous quartz dyke	90	16–98	47	
	Copper molybdenum porphyry	120	98–526	331	

## 5.2. Aeromagnetic Anomaly Characteristics of Typical Magnetite

### 5.2.1. Aeromagnetic Anomalies Related to Magnetite-Type Sedimentary Metamorphic Rocks

Aeromagnetic anomaly characteristics of sedimentary metamorphic magnetite generally have high amplitudes, large gradients, and regular shapes in the study region. There are three typical abnormal shapes in the plane. The shapes are wide strips, narrow strips, and gourd shapes, and they reflect ore bodies of different sizes, shapes, and occurrences. We should monitor the aeromagnetic anomalies in metamorphic rock strata if these anomalies have the above characteristics and are consistent with the stratum occurrence.

Aeromagnetic anomaly C1 was caused by iron ore in the southwestern part of the study region. On the section map of aeromagnetic  $\Delta T$ , it is located against the background of a regional negative magnetic anomaly and presents multipeak anomalies. The abnormal curve of the main peak is regular and sharp. The two wings are narrow and basically symmetrical. The maximum amplitude of the anomaly is 2017.0 nT. Multiple survey lines have obvious responses on the section map. This indicates that anomaly C1 is true and reliable. On the map of aeromagnetic  $\Delta T$ , the anomaly shows a banded shape with near-NE trending (Figure 4a). It is surrounded by reduced magnetic anomalies. On the reduction to the pole of aeromagnetic  $\Delta T$  (Figure 4b), multipeak anomalies trending northeast are more intuitive. The coverage area on the plane is approximately  $2.8 \times 1.1 \text{ km}^2$ . There is still an obvious reflection on the map of the first vertical derivative of reduction to the pole of aeromagnetic  $\Delta T$  (Figure 4c). This corresponds to a significant local positive magnetic anomaly trending NE, indicating that the anomaly is caused by shallow magnetic bodies. This is consistent with the known burial depth of the ore body.

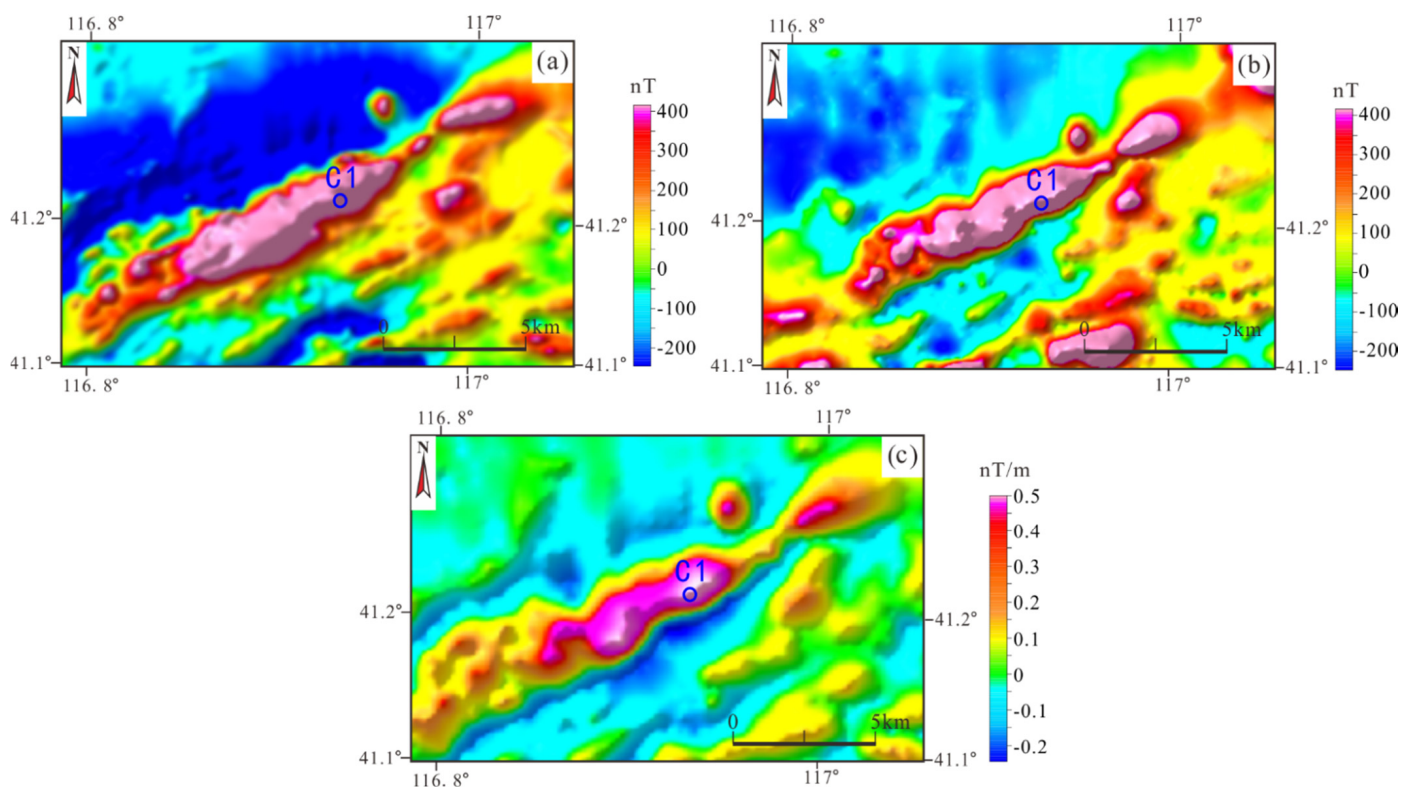


**Figure 4.** Aeromagnetic anomaly and its conversion of a sedimentary metamorphic magnetite in the study area: (a) Aeromagnetic data  $\Delta T$ , (b) reduction to the pole of aeromagnetic data  $\Delta T$ , (c) the first vertical derivative of reduction to the pole of aeromagnetic data  $\Delta T$ .

According to the 1:200,000 structural construction map (Figure 1), the Dantazi group of the Neoproterozoic was exposed on the surface at the center of the anomaly. Neoproterozoic tonalite gneiss is distributed in the northeast corner of this anomaly. A fault is developed in the north and south. The Baimiao Formation of the Dantazi group is a set of intermediate regional metamorphic rock series. The main rock assemblages are biotite (hornblende) plagioclase gneiss, biotite plagioclase (monzonite) granulite, intercalated amphibolite, magnetite quartzite, phosphorus bearing iron plagioclase hornblende diopside, plagioclase shallow granulite, and meta granulite. The rock formation has undergone strong migmatization. It represents an important occurrence horizon and wall rock of Anshan-type sedimentary metamorphic magnetite.

According to the measured physical (magnetic) data, the average magnetic susceptibility of the Neoproterozoic gneiss is  $495 \times 10^{-5}$  SI. Generally, it shows medium–weak magnetism. The surrounding rocks of Wuyingzi magnetite are gneiss and plagioclase amphibolite with magnetite. Physical property data show that the magnetic susceptibility of the wall rocks can reach  $41,293 \times 10^{-5}$  SI. The magnetic susceptibility obviously increases near the ore body. A high-amplitude aeromagnetic anomaly is caused by sedimentary metamorphic iron ore with strong magnetism.

#### 5.2.2. Aeromagnetic Anomalies Related to Magnetite-Type Magmatic Rocks

Iron ores of this type are mostly distributed in ultrabasic and basic rock belts controlled by deep and large faults. On aeromagnetic maps with a scale of 1:50,000 or 1:25,000, basic and ultrabasic rocks with a certain scale often cause local high-value aeromagnetic anomalies. We can further decompose the aeromagnetic anomalies of large-scale rocks. Superimposed magnetic anomalies with high amplitude often have a small range in the background of large rock masses. These magnetic anomalies are mostly caused by the ore body of vanadium titanium magnetite, ore body of iron phosphorus, or mineralized body. Therefore, in the distribution area of ultrabasic and basic rock masses, rocks with magnetic anomalies of local high amplitude in the background magnetic field should be considered reflections of iron ore or mineralized bodies. There are concealed rock bodies in deep and large fault zones.

Aeromagnetic anomaly C2 was caused by iron ore of magmatic type in the southwestern part of the study region. On the section map of aeromagnetic  $\Delta T$ , it is a unimodal anomaly against a negative background. The abnormal curve is regular and sharp. The two wings are narrow and basically symmetrical. The maximum amplitude of the anomaly is 910.7 nT. Multiple survey lines have obvious responses on the section map. This indicates that anomaly C2 is reliable. On the map of aeromagnetic  $\Delta T$ , the anomaly shows a near-elliptical anomaly with a long axis in the near-EW direction (Figure 5a). The contours are dense to the north and west of the anomaly, on the reduction to the pole of aeromagnetic  $\Delta T$  (Figure 5b). The anomaly shows a spike anomaly in the rising positive background. The coverage area is approximately  $1.0 \times 0.8 \text{ km}^2$  on the plane. There is still an obvious reflection on the map of the first vertical derivative of reduction to the pole of aeromagnetic  $\Delta T$  (Figure 5c).

According to the 1:200,000 structural construction map (Figure 1), the anomaly is located near the contact zone between the Neoproterozoic tonalite gneiss and the Baimiao Formation of the Dantazi group. According to the measured physical (magnetic) data, the average magnetic susceptibility of the Neoproterozoic gneiss is  $495 \times 10^{-5}$  SI in this region. Generally, the magnetism is not high. It cannot cause such a high-amplitude aeromagnetic anomaly. The high-amplitude aeromagnetic anomaly is caused by magmatic magnetite with strong magnetism.

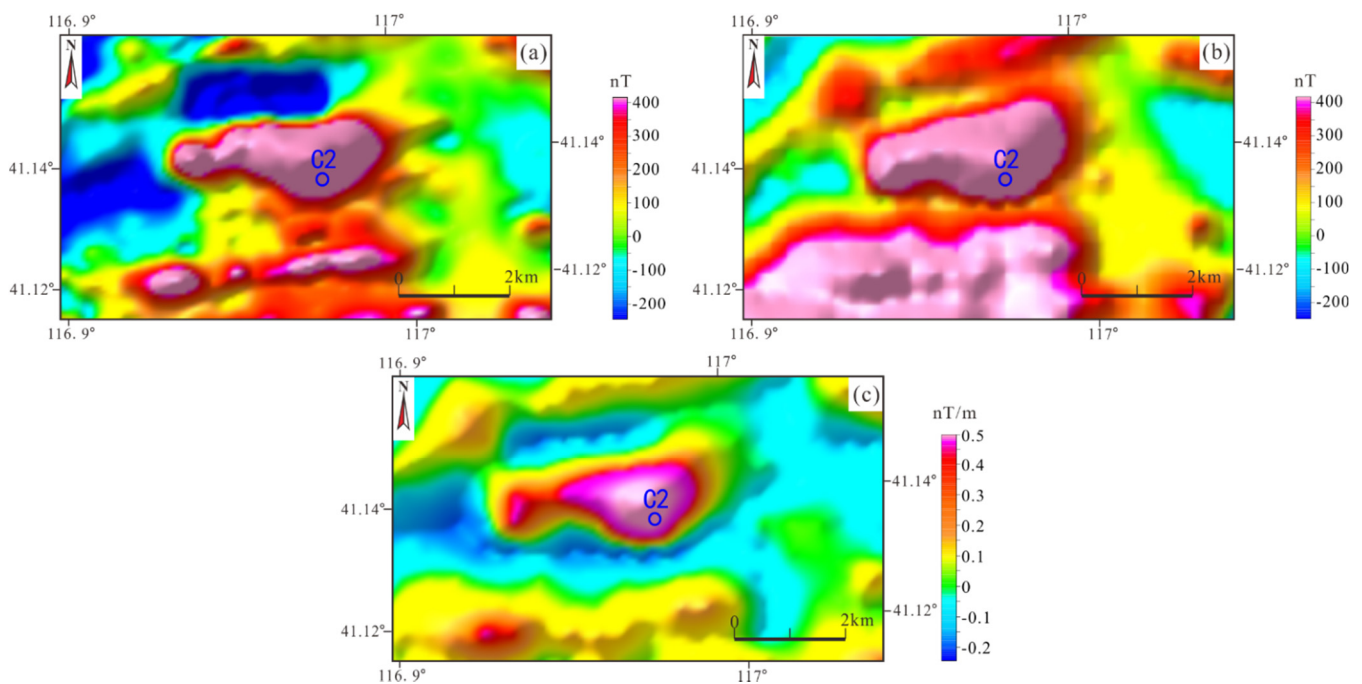


**Figure 5.** Aeromagnetic anomaly and its conversion of some magmatic rock magnetite in the study area: (a) Aeromagnetic data  $\Delta T$ , (b) reduction to the pole of aeromagnetic data  $\Delta T$ , (c) the first vertical derivative of reduction to the pole of aeromagnetic data  $\Delta T$ .

## 6. Magnetite Prospecting Prediction of Aeromagnetic

### 6.1. Prospect Attributes

Certain types of deposits are related to certain strata, structures, and magmatic rocks. They form a response with certain aeromagnetic anomaly characteristics. Based on the comparative analysis of the metallogenic background, aeromagnetic anomalies, and other characteristics of known deposit types, we summarize the prospecting attributes of sedimentary metamorphic and magmatic magnetite.

#### 6.1.1. Sedimentary Metamorphic Magnetite

##### (1) Geological attributes

- a. Most of the ore occurrences are regions in basement uplift with exposure of magnetic basement (Neoproterozoic and Paleoproterozoic) or covering of thin Cenozoic. However, the negative structure is more conducive to preserving ore bodies. In particular, the regions of syncline axes and turning ends often have large-scale and thick ore bodies.
- b. The Dantazi group of the Neoproterozoic is the main ore-bearing strata. The surrounding rocks of the deposit are various plagioclase gneiss, granulite, and granulite. The ore beds are mostly magnetite quartzite or magnetite amphibolite. The shapes are layered, stratoid, or lenticular. This occurrence is basically consistent with the surrounding rocks.
- c. The prospecting region is mainly located in the southern part of the study region, including southern Fengning County, southern Longhua County, and northern Luanping County in the Chengde area. Ore bodies mostly occur with the types in groups and zones. The strike direction of ore bodies mainly includes the near-EW directions. They are closely related to near-EW trending faults.

##### (2) Aeromagnetic attributes

- a. Sedimentary metamorphic magnetite is mainly located in magnetic anomaly areas alternating between positive and negative.

- b. The shape of the magnetic anomaly is regular in the plane, mostly in the strip, oval and gourd directions. The long axis direction of the abnormality is mostly consistent with the strike of the metamorphic strata of the ore body. Most of the shapes of abnormal sections peaked. The side with a gentle gradient is consistent with the formation tendency.
- c. The combination of ore-induced magnetic anomalies is mostly distributed alternately in the form of intermittent banded or beaded positive magnetic anomalies. They are mainly in the near-EW direction. Very few show a near-NE direction.
- d. The amplitude of the magnetic anomaly changes greatly. High amplitudes of local magnetic anomalies often reflect exposed ore bodies or bodies that are near the surface.
- e. Using the method of upward continuation, the amplitude of the anomaly caused by magnetite decreases sharply with increasing upward continuation height.

### 6.1.2. Magmatic Magnetite

#### (1) Geological attributes

- a. The prospecting region is mainly located in large fault zones of grade I, grade II, and their surroundings in the study area.
- b. The ore body is mainly composed of vanadium, titanium, and ilmenite. It contains a small amount of chromite, pyrite, chalcopyrite, apatite, etc. The metallogenic rocks are mainly basic rocks of gabbro, norite, and anorthosite. The secondary rocks are ultrabasic rocks of hornblende and pyroxenite.
- c. The ore body is an iron deposit of late penetrating magma. Iron ore deposits occur in groups under the control of structural fracture zones, contact zones of different lithofacies (gabbro and anorthosite contact zones), and primary structures.

#### (2) Aeromagnetic attributes

- a. The linear gradient belt of magnetic anomalies with a large scale reflects the deep and large fault zone. Local magnetic anomalies with high amplitudes reflect the ultrabasic and basic rocks containing magnetite.
- b. The magnetic anomaly has an obvious superposition phenomenon. A positive magnetic anomaly of a large background region is caused by an ultrabasic and basic rock mass. The local closed anomaly with high amplitude superimposed on the background is a mine-induced anomaly.
- c. The shapes of magnetic anomalies reflecting the rocks and ore body are mostly elliptical and massive.
- d. Ore-induced magnetic anomalies with high amplitudes reflect closely arranged and centrally distributed ore bodies.
- e. If the concealed depth of rocks and ore body is large, it is difficult to distinguish them by using only an isoline plan or profile of aeromagnetic anomaly  $\Delta T$ . Upward continuation should be used. The ore anomaly decays rapidly if the height of upwards extension increases.

### 6.2. Magnetite Prediction Method

Based on the lithology and structural characteristics reflected by aeromagnetic data, combined with regional magmatic activity, metallogenic type, and metallogenic environment, we divided and evaluated prediction regions of ore prospecting based on a detailed analysis and summary of known deposit geology, geophysical characteristics, geochemical characteristics, and the establishment of prospecting attributions.

The specific division principles of the prospecting prediction regions are as follows: the metallogenic geological conditions are very favorable. There are known deposits distributed in the region. The geological and aeromagnetic attributions of prospecting are obvious. The anomalies with prospecting significance are developed in groups or distributed in large quantities. The results of forward calculation and resource prediction show the great potential for finding new ore bodies or further exploration. According to the

above principles, we divided the six prospecting prediction regions into the entire study region (Figure 6).

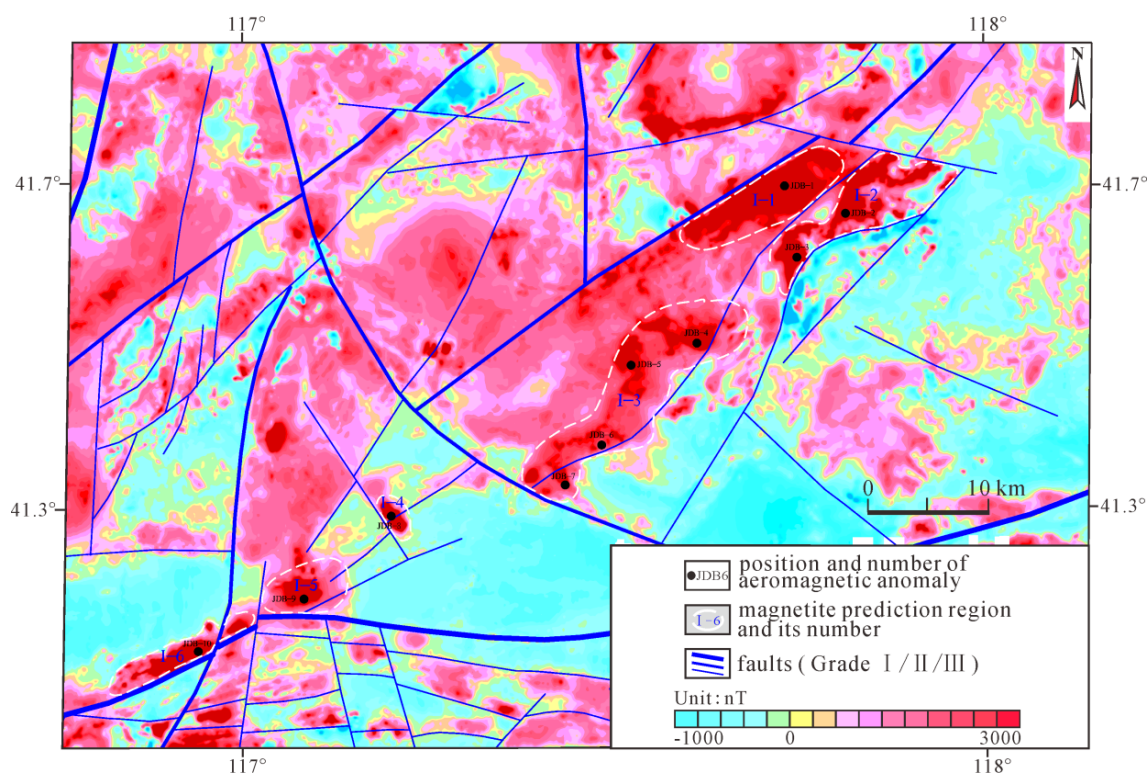


**Figure 6.** Reduction to the pole of aeromagnetic data  $\Delta T$  and magnetite prediction region in northeast Hebei: I-1: Ore prediction region of iron polymetallic in Laochenjia, I-2: Iron ore prediction region of Dabai-Henan, I-3: Iron ore prediction region of Jiuwuying-baiyingzi, I-4: Ore prediction region of iron polymetallic in Beierying, I-5: Ore prediction region of iron polymetallic in Sidaogoumen, I-6: Ore prediction region of iron polymetallic in Wuyingzi.

In view of the differences in the metallogenic, geological, tectonic, and magmatic environments and their aeromagnetic responses, the six prospecting prediction regions have different characteristics. The main evaluations are as follows:

#### 6.2.1. Ore Prediction Region of Iron Polymetallic in Laochenjia (I-1)

It is located in the northeastern part of the study region and is distributed with a near-NE-trending strip shape. The distribution area is approximately 98.3 km<sup>2</sup>. Mesozoic granite and Neoproterozoic metamorphic rocks are exposed in the north. The Zhangjiakou Formation of the Jurassic is widely exposed in the south. The aeromagnetic map (Figure 6) shows a magnetic anomaly zone with local positive and high values superimposed on the positive magnetic background. The maximum abnormal value reached 959.8 nT (Figure 6). During the field survey, we found four ore spots in the prediction area, including one magnetite, two gold mines, and one lead-zinc mine. The ground investigation of aeromagnetic anomalies infers that positive magnetic anomalies with high amplitudes are mostly caused by iron ore. Based on comprehensive geophysical and geochemical exploration data, this region is a prediction area for looking for iron polymetallic deposits.

#### 6.2.2. Iron Ore Prediction Region of Dabai-Henan (I-2)

Adjacent to the prediction region of Laochenjia on the west side, it is distributed in a NE-trending strip. The distribution area is approximately 129.0 km<sup>2</sup>. The Jurassic Dabeigou Formation is widely exposed on the surface. Local regions in the southwestern part are covered by Quaternary deposits. On the aeromagnetic map (Figure 6), there are two large

background positive magnetic anomalies. One anomaly is NE-trending (in the northern part). The other is nearly N–S-trending (in the southern part). The results of the ground investigation show that positive magnetic anomalies with high amplitudes are caused by concealed magmatic rocks. Based on the comprehensive geophysical exploration data and ground investigation of aeromagnetic anomalies, we infer that this region is a favorable region for searching for magmatic magnetite.

### 6.2.3. Iron Ore Prediction Region of Jiuwuying-Baiyingzi (I-3)

It is located along the line of Jiuwuying-Yingtaogou-Baiyingzi in the middle of the study region with a near-S shape. The distribution area is approximately 210.6 km<sup>2</sup>, and Mesozoic granites and Neoproterozoic metamorphic rocks are widely exposed on the surface. The Zhangjiakou Formation of the Jurassic is exposed on the eastern margin. The aeromagnetic map (Figure 6) corresponds to local high magnetic anomalies in the positive magnetic background. During the field survey, we found three magnetite mining sites in the prediction area. The results of aeromagnetic anomaly ground investigation show that the high-amplitude magnetic anomaly is mostly caused by ultrabasic rocks containing vanadium titanomagnetite. Based on geophysical and geochemical data, this region is a prediction area for seeking iron polymetallic deposits.

Taking the anomaly JDB-4 in the northeast of the prediction area as a case, the long axis of the anomaly is a near-elliptic shape with a near-NE trend on the plane (Figure 7a,b). The contour lines are dense. The scale is approximately 4.0 × 2.4 km<sup>2</sup> on the plane. The maximum anomaly value is 578.4 nT. There is still an obviously high value on the map of the first vertical derivative of reduction to the pole of aeromagnetic data  $\Delta T$  (Figure 7c). Using the method of upward continuation, the amplitude of the anomaly caused by magnetite decreases sharply with increasing upward continuation height (Figure 7d). Based on the aeromagnetic data, we calculated the depths causing the anomaly JDB-4 using the Euler deconvolution (Figure 7e). The computing size of window was 15. We comprehensively consider the magnetism of the rocks and stratum according to the field physical parameters (Table 1). We comprehensively consider the magnetism of the rocks and stratum according to the field physical parameters (Table 1). The result shows that the depth values of the magnetic body are mostly less than 1 km and partly smaller than 0.5 km, indicating the magnetic body causing the anomaly JDB-4 being shallow, which is consistent with the interpretation from the upward continuation (Figure 7e).

The anomaly is located near the contact zone between porphyritic alkaline granite of the Early Cretaceous and the Dantazi group of the Neoproterozoic. There is a near-NE-trending fault on the side.

During the field anomaly survey, we found mineralization outcrops of magmatic magnetite under the Cretaceous volcanic rocks (Figure 7f). During ground verification, the geomagnetic profile (line NO. 223) (Figure 8) was arranged at the maximum value of the aeromagnetic anomaly. The results show that the geomagnetic anomaly curve also has an obviously high amplitude. The gradient of the original curve is similar on both the northwest and southeast sides. The anomalies on the northwest side tend to be faster in the background field, while the anomalies on the southeast side are slower. The maximum anomaly value is 4510 nT. The depolarization anomaly curve is slow in the southeast and steep in the northwest. There is a negative anomaly with a small amplitude on the southeast side. The anomalies in the northwest side tend to be in the background field. Euler solutions are concentrated in the region where there are magnetic differences between magnetite bearing ultrabasic rocks and their surrounding rocks. According to the profile curve, we inferred that the buried magnetic body steeply inclined to the northwest. The center of the anomaly is consistent with the ultrabasic rocks exposed on the surface. Combined with magnetic measurement results of field rock samples, we inferred that the anomaly is caused by biotite hornblende gabbro containing vanadium and titanium. The test results of ore samples collected from ultrabasic rocks show that the iron and titanium contents of the sorted samples have reached industrial grade.

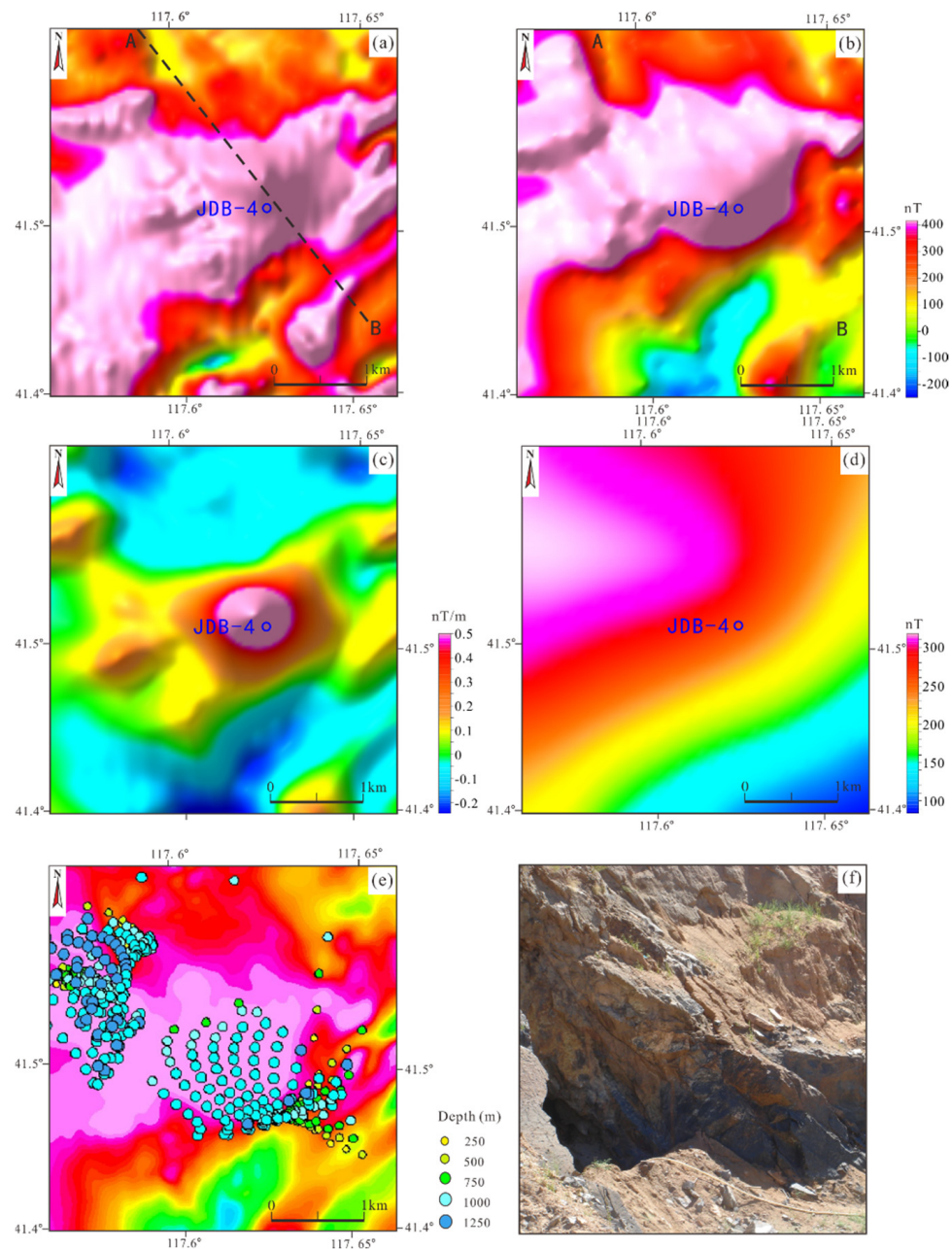


**Figure 7.** Aeromagnetic anomaly JDB-4 and its corresponding magnetite deposit: (a) Aeromagnetic data  $\Delta T$ , (b) reduction to the pole of aeromagnetic data  $\Delta T$ , (c) the first vertical derivative of reduction to the pole of aeromagnetic data  $\Delta T$ , (d) reduction to the pole of aeromagnetic anomaly (upwards extending 3 km), (e) depth by Euler deconvolution, (f) photograph of iron deposit mined. A–B are the locations of the section shown in Figure 8.

This aeromagnetic anomaly has a large scale. It is the comprehensive response of ultrabasic rocks with high magnetism and density. These iron-bearing ultrabasic rocks have a certain scale in depth. The abnormal area is a favorable region for searching magmatic iron ore.

Let us take another case of anomaly JDB-7 at the southern corner of this region. It is located at the transition position in the interphase regions of the large-scale aeromagnetic positive and negative anomalies (Figure 6). The anomaly has a regular shape. The long axis of the anomaly has a near-elliptic shape with a near-NW trend on the plane (Figure 9a,b). The contours are dense. The coverage area is approximately  $1.0 \times 0.8 \text{ km}^2$  on the plane. The

maximum amplitude is 940.4 nT. On the map of the first vertical derivative of reduction to the pole of aeromagnetic  $\Delta T$  (Figure 9c), the anomaly shows an obvious and local positive magnetic anomaly with a NW trend. During surface exploration, we found sedimentary magnetite mineralization at the surface position corresponding to the anomaly (Figure 9d).

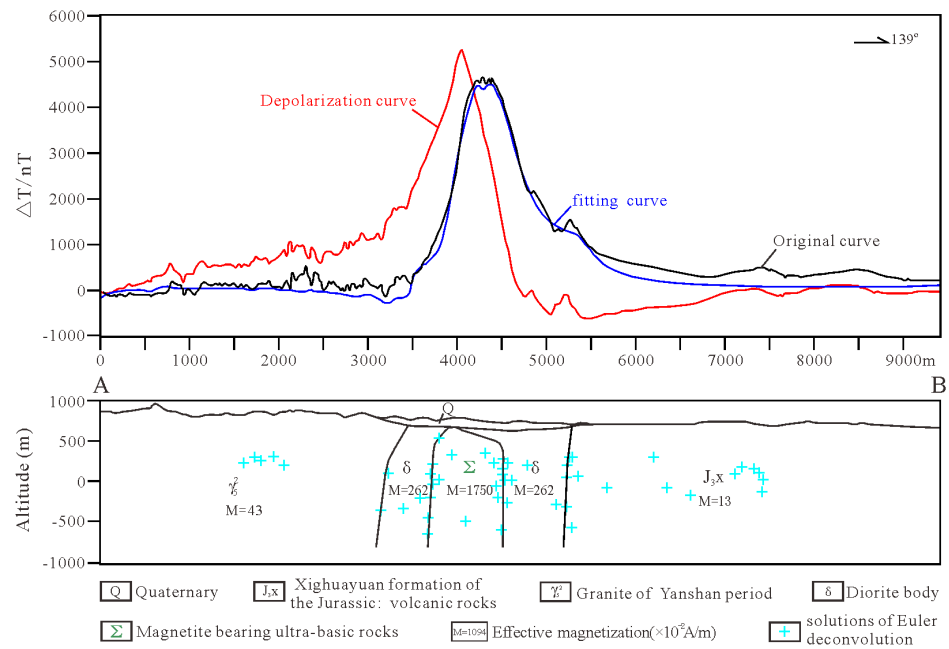


**Figure 8.** Magnetic data  $\Delta T$  profile of the ground survey (line NO. 223). The location of the line is shown in Figure 7a.

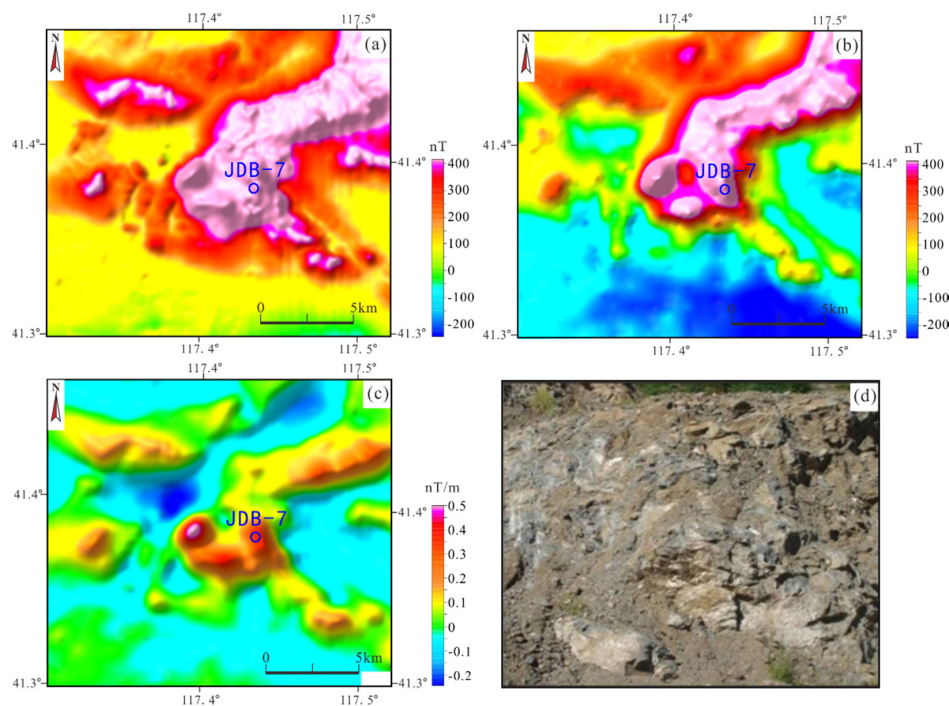


**Figure 9.** Aeromagnetic anomaly JDB-7 and its corresponding magnetite deposit: (a) Aeromagnetic data  $\Delta T$ , (b) reduction to the pole of aeromagnetic data  $\Delta T$ , (c) the first vertical derivative of reduction to the pole of aeromagnetic data  $\Delta T$ , (d) photograph of iron deposit mined.

#### 6.2.4. Ore Prediction Region of Iron Polymetallic in Beierying (I-4)

The Neoproterozoic metamorphic rocks exposed on the surface of the prediction region. Mesozoic granites are exposed in the surrounding region. The aeromagnetic  $\Delta T$  map shows a local high magnetic anomaly on the background of magnetic fields with positive and negative changes (Figure 6). During the field anomaly survey, we found seven ore occurrences near the prediction region, including three magnetites, one lead-zinc mine, two gold mines, and one molybdenum mine. The results of aeromagnetic anomaly ground investigation show that the high-amplitude magnetic anomaly is mostly caused by magnetite in porphyritic migmatites. Based on comprehensive geophysical and geochemical data, this area is a prediction region for seeking iron polymetallic deposits (iron, lead, zinc, and gold).

On the map of aeromagnetic  $\Delta T$  (Figure 10a), anomaly JDB-8 shows multipic anomalies in a flat positive anomaly background. The abnormal curve is regular and sharp. The two wings are narrow and basically symmetrical. An associated negative anomaly developed in the northeast of anomaly JDB-8 (Figure 10a). There are three secondary anomalies developed in the northwest, southeast, and south of the anomaly (Figure 10b). The abnormal amplitude is between 700 and 2330 nT. On the first vertical derivative of reduction to the pole of aeromagnetic  $\Delta T$  (Figure 10c), the long axis of the anomaly is a near-elliptic shape with a near-NE trend on the plane. The anomaly contours are dense and still have obvious anomalies. Based on the aeromagnetic data, the depths of the magnetic bodies causing the anomaly JDB-8 were calculated using the Euler deconvolution (Figure 10d). The result shows that the values of depth are mostly less than 0.25 km in the north and mostly between 0.5 and 1.0 km in the south, indicating the magnetic body causing the anomaly JDB-8 being shallow, which is consistent with the qualitative interpretation of the preceding upward continuation.

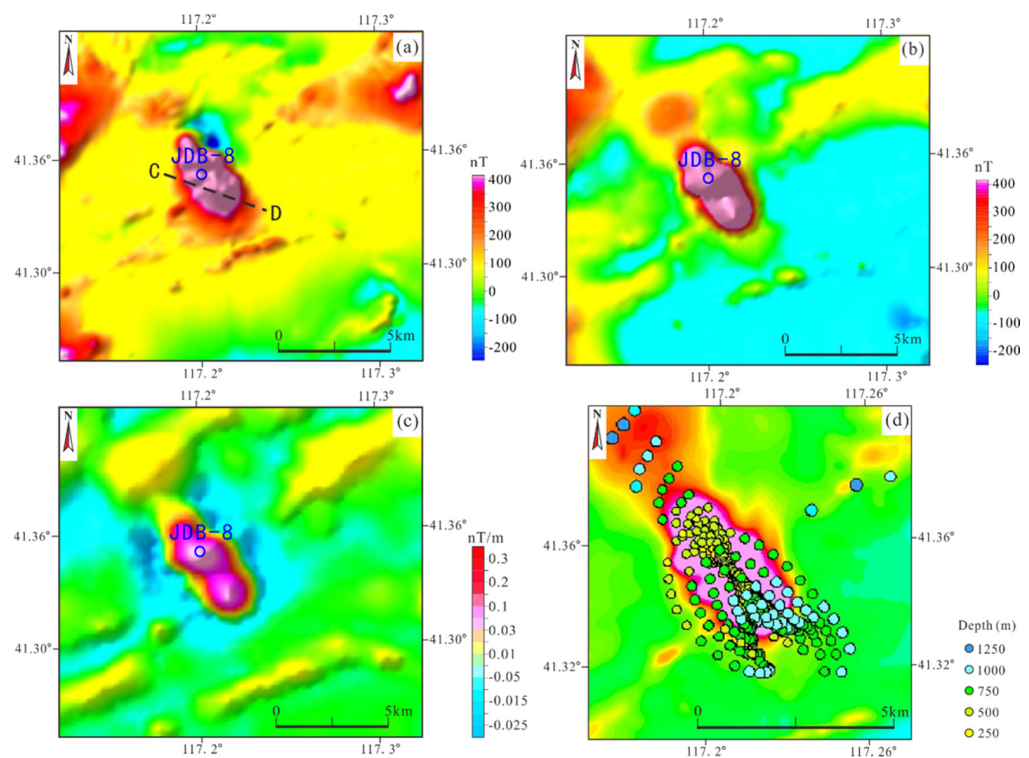


**Figure 10.** Aeromagnetic anomaly JDB-8 and its conversion: (a) Aeromagnetic data  $\Delta T$ , (b) reduction to the pole of aeromagnetic data  $\Delta T$ , (c) the first vertical derivative of reduction to the pole of aeromagnetic data  $\Delta T$ , (d) depth by Euler deconvolution.

According to the 1:200,000 structural construction map (Figure 1), the anomaly is located near the contact zone between metamorphic porphyry monzogranite of the Paleoproterozoic, metamorphic granodiorite of Paleoproterozoic, and syenogranite (Potassic feldspar granite) of the late Permian. NE-trending faults are developed in the south and northeast of the anomaly. Based on the measured physical (magnetic) data, the average magnetic susceptibility of the Paleoproterozoic gneiss is  $148 \times 10^{-5}$  SI in this region. Generally, the magnetism is not high. The average magnetism of the syenogranite (Potassic feldspar granite) in the late Permian is  $603 \times 10^{-5}$  SI. The results of the aeromagnetic anomaly ground investigation show that the locations of the aeromagnetic and geomagnetic anomalies are very consistent (Figures 10a and 11c). There are two obvious IP anomalies distributed in this region (Figure 11b). The left anomaly shows low resistance and high polarization. The right anomaly shows high resistance and high polarization. On the cross-section of the isoline of relative strength, the apparent polarizability of fixed-point source sounding ( $\eta_s$ ) shows a relatively high-amplitude anomaly inclined to the southeast side (in the middle of the section). The anomaly characteristics are consistent with the IP anomaly at the corresponding location. The inversion resistivity profile of controllable source audio magnetotelluric sounding shows that there is a nearly vertical and low resistivity zone with a funnel shape between elevations from 800 to 100 m (Figure 10c,d). This is consistent with the magnetic and IP anomalies in the middle of the section. It reflects the distribution characteristics of mineralized bodies of metal sulfide and magnetite. The results of the forward and inversion methods of 2.5 D optimization fitting show that the near vertical and high resistivity zones may be caused by magmatic intrusion (Figure 11c). An altered fracture zone was found near the anomaly during the ground survey. During the field anomaly survey, we found an altered fracture zone with cristobalite mineralization and pyritization. The zone is narrow at the top and wide at the bottom. It has a thickness of 0.8–1.2 m. The attitude is  $205^\circ \angle 84^\circ$ . The laboratory test results of the test block sample are  $23,751 \times 10^{-6}$  (Pb),  $222.8 \times 10^{-6}$  (Zn),  $121.8 \times 10^{-6}$  (Cu), and  $114 \times 10^{-9}$  (Ag).

Based on the characteristics of the aeromagnetic anomaly (Figure 10a), magnetic anomaly of the ground survey, IP medium gradient anomaly, anomaly of fixed-point source sounding, anomaly of controllable source audio magnetotelluric sounding, and element (Ag and Pb) anomaly of the soil survey (Figure 11), the result shows that the overall magnetic anomaly of Beierying reflects the intrusion of large-scale magmatic rocks with strong magnetism. In the geochemical figure of silver and lead elements measured in the soil (Figure 11a), there are two anomalies of silver and lead, respectively, in the line. The anomalies of silver and lead in the southwest are in suitable agreement. However, the scale of silver element corresponding anomaly is relatively small. The anomalies of silver and lead elements coincide well in the southeast. The scale is large and the content is high. The data of two element concentration centers show that the maximum content of silver is  $1.61 \times 10^{-6}$ , and the maximum content of lead is  $246.9 \times 10^{-6}$ . The concentration centers of lead and silver are in suitable agreement with the IP and magnetic anomaly. The local geomagnetic  $\Delta T$  anomaly with high amplitude (the maximum value is 21,000 nT) indicates the existence of strong magnetic geological bodies. Local anomalies of polymetallic IP and geochemical (anomalies of Ag and Pb from soil measurements) should be caused by late hydrothermal solutions, including sulfides. There generally had Euler solutions where there are magnetic differences between the inferred magnetite bodies and their surrounding strata. This region is a favorable area for searching magnetite and even polymetallic mines. This suggests that it should be verified as soon as possible.

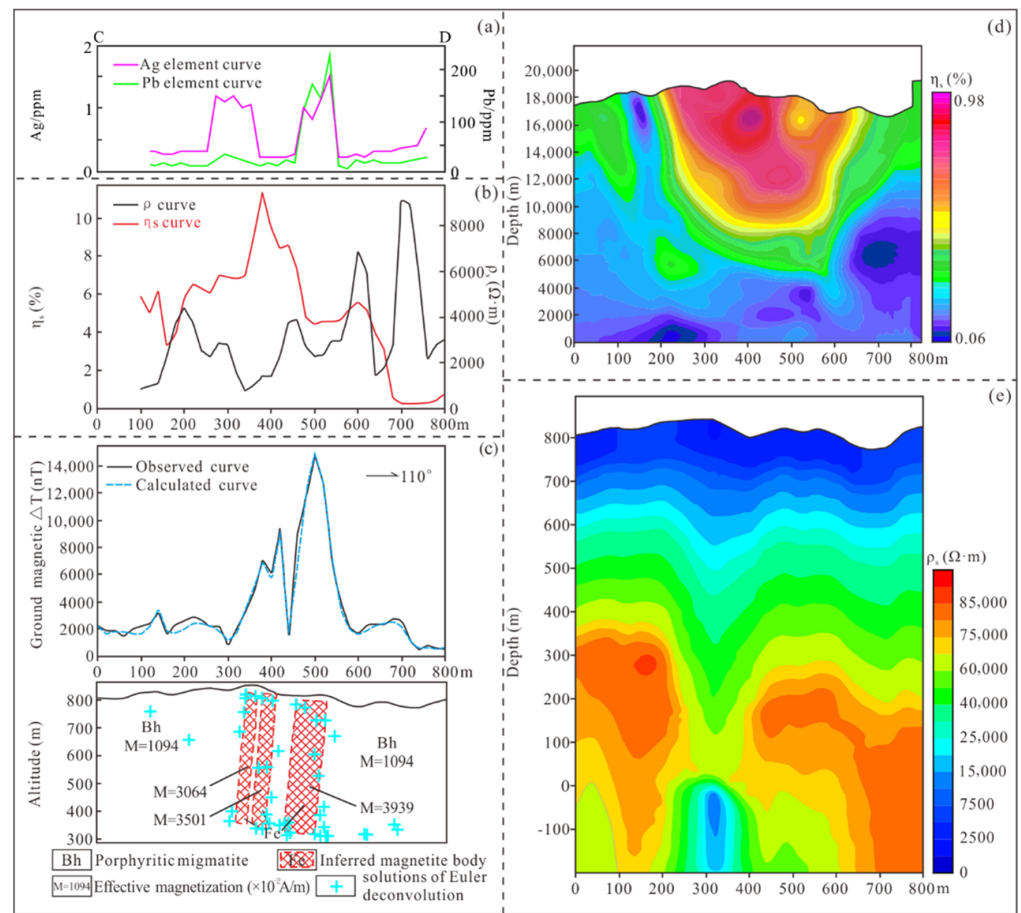


**Figure 11.** Integrated geophysical profiles of ground surveying of anomaly JDB-8: (a) anomalies of Ag and Pb from soil measurements, (b) curve of IP central gradient method of ground surveying line 2, (c) forward fitting profile to magnetic data  $\Delta T$  of ground surveying line 2, (d) profile of  $\eta_s$  relative intensity by fixed-source sounding for ground surveying line 2, (e) CSAMT inversion resistivity profile.

### 6.2.5. Ore Prediction Region of Iron Polymetallic in Sidaogoumen (I-5)

The prediction region is in the southwestern part of the study region. The shape of this anomaly is nearly elliptical, with an area of approximately 50.2 km<sup>2</sup>. Metamorphic quartz diorites of the Neoproterozoic and metamorphic rocks are exposed in the middle and south. Zhangjiakou Formation of the Jurassic is exposed in the local sections. The aeromagnetic  $\Delta T$  map (Figure 6) shows a local positive magnetic anomaly with an irregular shape in the negative magnetic field background.

There are six ore occurrences near the prediction region, including three magnetites, two gold mines, and one molybdenum mine. The results of the aeromagnetic anomaly ground investigation show that the high-amplitude magnetic anomaly is mostly caused by magnetite. According to the aeromagnetic geomagnetic and geochemical anomalies, we concluded that this area is a favorable region for searching for supergrade iron ore, gold mines, and polymetallic mines.

### 6.2.6. Ore Prediction Region of Iron Polymetallic in Wuyingzi (I-6)

This prediction region is in the southwestern part of the study region. It is distributed in a narrow strip in a near-NE trend with an area of approximately 55.9 km<sup>2</sup>. The metamorphic quartz diorites of the Neoproterozoic and the metamorphic rocks are widely exposed on the surface. The Mesoproterozoic granites are exposed in the local sections of the southwest margin. It shows a magnetic anomaly of a local positive band in the negative magnetic field background on the aeromagnetic  $\Delta T$  map (Figure 6).

There are four ore occurrences near the prediction region, including one magnetite, two gold mines, and one molybdenum mine. The ground investigation results of the aeromagnetic anomaly show that this area is a favorable region for searching for supergrade iron ore, gold mines, and polymetallic mines.

Anomaly JDB-10 is in the southwestern part of the study region. The long axis of the anomaly is a near-elliptical shape with a near-NE trend on the plane (Figure 12a). The anomaly contours are dense. The coverage area on the plane is approximately  $2.1 \times 1.1 \text{ km}^2$  (Figure 12b). This anomaly still has obvious reflection on the map of the first vertical derivative of reduction to the pole of aeromagnetic  $\Delta T$  (Figure 12c). Based on the aeromagnetic data, we calculated the depths of the magnetic bodies causing the anomaly JDB-10 using the Euler deconvolution (Figure 12d). The result shows that the values of depth are mostly less than 1 km and partly smaller than 0.25 km, and greater in the west (mostly greater than 1 km) and smaller in the east (mostly less than 750 m).

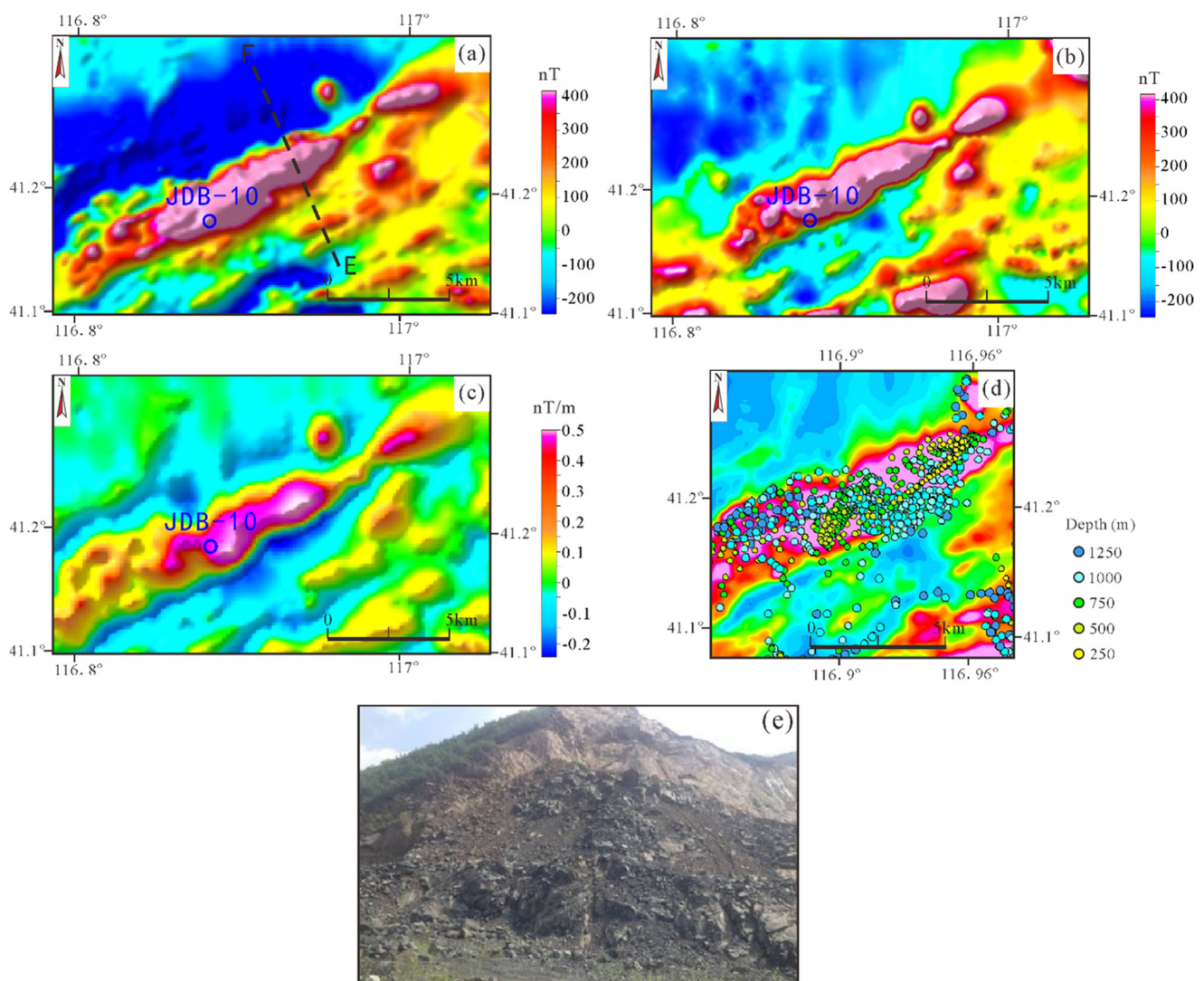


**Figure 12.** Aeromagnetic anomaly JDB-10 and its corresponding magnetite deposit. (a) Aeromagnetic data  $\Delta T$ , (b) reduction to the pole of aeromagnetic data  $\Delta T$ , (c) the first vertical derivative of reduction to the pole of aeromagnetic data  $\Delta T$ , (d) depth by Euler deconvolution, (e) photograph of iron deposit mined. E-F are the locations of the section shown in Figure 13.

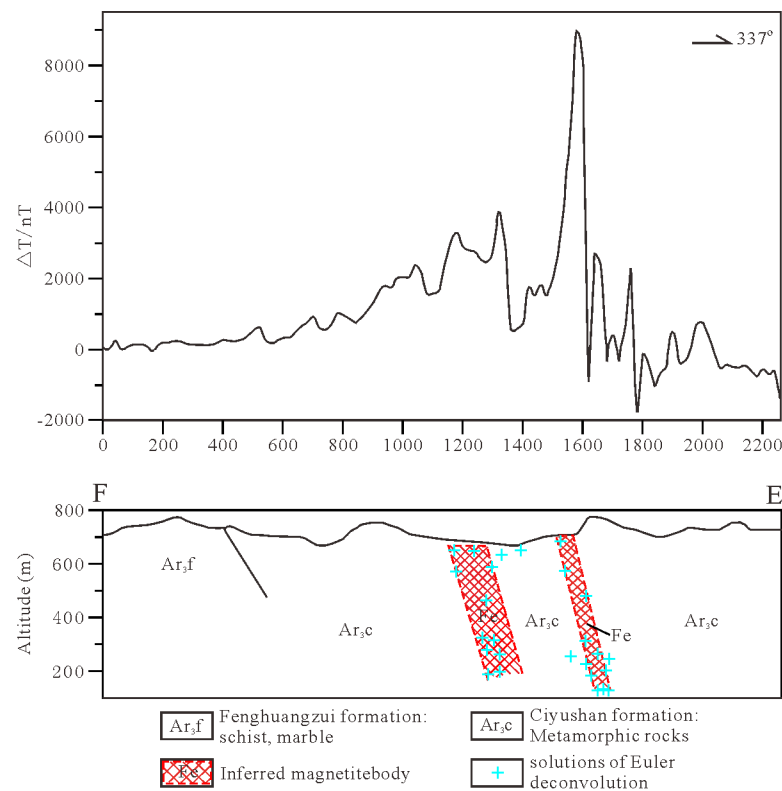


**Figure 13.** Magnetic data  $\Delta T$  profile of the ground survey (line NO. 227).

During ground verification, two geomagnetic lines are arranged at the maximum value of the aeromagnetic anomaly. The magnetic anomaly of the profile curve generally has a large gradient and high amplitude (Figure 13). Magnetic anomalies in adjacent sections are regular. The magnetic anomaly of the No. 227 line shows three peaks. The maximum anomaly value is 8560 nT. The anomaly has a large gradient on the northwest side and a slow gradient on the southeast side. Euler solutions are concentrated in the region where there are magnetic differences between inferred magnetite bodies and their surrounding strata. According to the profile curve, the magnetic body is steeply inclined to the southeast. This large-scale anomaly is located on the sedimentary, metamorphic magnetite belt in Yunwushan-Wangying of Fengning. During surface exploration, we found an outcrop with mineralized iron (Figure 12e). It is concluded that the anomaly is caused by sedimentary metamorphic magnetite and has great prospecting potential.

## 7. Discussion and Conclusions

### 7.1. Discussion

- (1) From the regional geological mineral figures (Figure 1) and aeromagnetic data  $\Delta T$  map (Figure 6), the line of Shangyi-Fengning-Longhua is a demarcated magnetite metallogenic boundary northeast of Hebei province. The southern region of this line (refer to southern region) belongs to the deep metamorphic rocks of the Archean and iron-rich region in eastern Hebei. Deep metamorphic rocks of the Archean are widely exposed in this region. Many large-scale sedimentary metamorphic-rich iron ores are distributed. Magnetites with mining values have not been found in the region between the north of the line and the northern margin of the North China block (referred to northern region). The sedimentary metamorphic and magmatic magnetite occurrences in this region need to be further studied. The regional distribution of stratigraphic, sedimentary-pyroclastic rock series of the Jurassic-Cretaceous and acid intrusive rocks of the late Paleozoic are widely distributed in the northern region. Medium-shallow metamorphic rocks of Neoproterozoic are exposed locally. They have

low magnetite content. It can be seen that the southern region has better metallogenic conditions for sedimentary metamorphic magnetites. We should pay more attention to the prospect in the deep and surrounding areas of the known mining areas. The northern region has better metallogenic conditions for gold, silver, lead, zinc, and molybdenum polymetallic deposits. We should pay further attention to this kind of mineral product.

- (2) From the characteristics of regional geology and mineral resources distribution, the fault zone in Shangyi-Fengning-Longhua plays an important role in controlling the metallogenic belt. Along the Shangyi-Fengning-Longhua fault zone, there are not only deep metamorphic rocks of the Archean and basic-ultrabasic intrusive rocks, but also sedimentary metamorphic and magmatic magnetites distributed in these belts. This important strata-structure-magmatic-magnetite belt reflects that the Shangyi-Fengning-Longhua fault is a deep fracture with large cutting depths and long extension distances, which should cut into the deep mantle. Therefore, the formation and evolution of this fault belt and its ore-controlling functions should be further studied.
- (3) It is very effective to identify correctly different characteristics of aeromagnetic anomalies for searching magnetites directly. Under normal conditions, the sedimentary rocks have no or weak magnetism. They often show negative magnetic anomalies or low-weak anomalies on the aeromagnetic map. The magnetic strengths of metamorphic rocks are different. The shapes of positive magnetic anomalies are mostly planes or blocks. Most intrusive rocks have certain magnetic properties. Their magnetic strengths are different because of the different lithologies. The shapes of positive magnetic anomalies are mostly perfectly round or belt. The volcanic rocks are mostly magnetic, but their magnetic strengths of them vary greatly. Most of them show positive magnetic anomalies with a marked jump. The magnetites have strong magnetic strengths and high anomaly amplitudes. It has significant differences from other magnetic anomalies. It is easy to be identified from the characteristics of magnetic anomalies. The kind of magnetites should be determined based on the geological background. For example, the sedimentary metamorphic magnetites are distributed in the geological background areas with deep metamorphic rock. The magmatic magnetites are distributed in the distribution regions with basic-ultrabasic intrusive rocks. In a few cases, there are similar aeromagnetic anomalies that belong to the reactions of different strata or lithologies. It can be determined in combination with the geological background.

## 7.2. Conclusions

- (1) The zone from Laochenjia to Wuyingzi has the metallogenic conditions of sedimentary, metamorphic, and magmatic iron deposits. More than 10 aeromagnetic anomalies with large scales and high amplitudes are developed in this region. It is one of the important aeromagnetic anomaly zones in northeastern Hebei. Combining the results of physical measurements and ground verification, aeromagnetic anomalies with high amplitudes are mainly caused by shallow magnetite deposits or ultrabasic rocks containing magnetite in this region. Therefore, the aeromagnetic anomalies with high amplitudes in Laochenjia, Daba-Henan, Jiuwuying, Baiyingzi, Beierying, Sidaogoumen, and Wuyingzi should be regarded as key prospecting targets.
- (2) Using methods of aeromagnetic reduction to pole, upward continuation, vertical derivative, conversion processing of residual anomaly data, and 2.5 D forward and inverse fitting, combined with geological outcrops, known iron deposits, ground magnetic surveys, and anomaly verification, we can carry out qualitative interpretation and quantitative calculation of magnetic bodies and then judge the distribution form and burial depth.
- (3) Based on the latest and measured aeromagnetic data with large areas and high precision, we can quickly screen aeromagnetic anomalies with prospecting significance. Based on high-precision aeromagnetic surveys, combined with geomagnetic meth-

ods, electrical methods, soil geochemistry, and other verification methods, it is an important way to realize accurate, rapid, and efficient ore prospecting.

**Author Contributions:** Data curation, Y.-X.L. and J.-W.Z.; Investigation, Y.-X.L., W.-Y.L., J.-W.Z., and C.Y.; Software, Y.-X.L. and L.-J.W.; Writing—original draft, Y.-X.L., W.-Y.L., A.-Q.C., and S.G.; Writing—review and editing, Y.-X.L., W.-Y.L., Z.-Y.L., and C.Y. All authors have read and agreed to the published version of the manuscript.

**Funding:** This work is supported by the Geological Exploration Foundation Project of Hebei of China (No. 30001200000224097) and the Geological Survey Project of China Geological Survey (No. 1212011220563; No. 12120114090401).

**Conflicts of Interest:** The authors declare that they have no conflict of interest.

## References

- Zhai, Y.S.; Yao, S.Z.; Cai, K.Q. *Mineral Deposits*; Geological Publishing House: Beijing, China, 2011; pp. 61–98.
- Cai, S.H.; He, H.Y.; Zhu, R.X. Magnetostratigraphic study of lower Cretaceous at Chengde Basin, Yanshan area and its restriction on North China Craton destruction. *Chin. J. Geophys.* **2012**, *55*, 66–75.
- Chen, C.L.; Jin, S.; Rong, G.L. Ore-controlling features of volcanic structure and prospecting potential in heshundian, Northern Hebei Province. *Geophys. Geochem. Explor.* **2011**, *35*, 461–467.
- Zhou, J.L.; Luo, Z.H.; Pan, Y.; Li, X.D. The genesis of vein-type iron orebody occurred in magmatic iron deposit: A case study of the Heishan iron deposit, Hebei Province, China. *Acta Petrol.* **2013**, *29*, 3555–3566.
- Hao, J.J.; Guo, H.Q.; Li, C.Z. The review and prospects of mineral exploration methods for the hanxing-type iron deposits in Hebei, China. *Geol. Surv. Res.* **2008**, *31*, 315–320.
- Sun, W.H.; Yang, J.L.; Li, H.J.; Liu, W.G.; Ma, S.J. Differences in properties between Pebbles and Raw ore from a SAG mill at a zinc, tin-bearing mine. *Minerals* **2022**, *12*, 774. [[CrossRef](#)]
- Zhang, Z.L.; Zhang, C.; Li, Y.; Wang, L.Y.; Gao, J.L.; Ma, M.; Li, Y.D. Petrogenesis and Geological Significance of the Quartz Monzonites in the Jinling Area, Western Shandong Province. *Minerals* **2022**, *12*, 771. [[CrossRef](#)]
- Jiang, S.H.; Liang, Q.L.; Bagas, L. Re–Os ages for molybdenum mineralization in the Fengning region of northern Hebei Province, China: New constraints on the timing of mineralization and geodynamic setting. *J. Asian Earth Sci.* **2014**, *79*, 873–883. [[CrossRef](#)]
- Li, H.M.; Li, L.X.; Zhang, Z.C. Alteration of the Damiao anorthosite complex in the northern North China Craton: Implications for high-grade iron mineralization. *Ore Geol. Rev.* **2014**, *57*, 574–588. [[CrossRef](#)]
- Li, L.X.; Li, H.M.; Che, Z.L. Hydrothermal mineralization and fluid inclusion study on the Heishan iron deposit, Chengde County, Hebei Province, China. *Acta Petrol.* **2010**, *26*, 858–870.
- Li, Z.H.; Zhu, X.K. Geochemical features of Xuanlong type iron ore deposit in Hebei Province and their geological significances. *Acta Petrol.* **2012**, *28*, 2903–2911.
- Liu, Y.X.; Li, W.Y.; Cao, A.Q. Recognition of Tuquan basin structure based airborne gravity magnetic characteristics. *Geol. Surv. China* **2018**, *5*, 44–50.
- Lu, Q.Q.; Luo, S.S.; Li, L.J. Sedimentary facies and geochemical characteristics of Mesoproterozoic Gaoyuzhuang Formation in Xuanlong Depression. *Fault–Block Oil Gas Field.* **2011**, *18*, 312–316.
- Chen, Z.L.; Chen, B.L.; Li, H.M.; Du, W.H.; Li, L.X.; Han, F.B.; Wang, Y.; Sun, Y.; Wu, Y.; Zhang, W.G. Geological Characteristics of the Damiao Iron Deposit, North China Craton and Ore-Prospecting. *Acta Petrol.* **2014**, *88*, 2339–2350.
- Bai, X.; Liu, S.W.; Wang, W. U-Pb geochronology and Lu-Hf isotopes of zircons from newly identified Permian-Early Triassic plutons in western Liaoning Province along the northern margin of the North China Craton: Constraints on petrogenesis and tectonic setting. *Int. J. Earth Sci.* **2013**, *102*, 671–685. [[CrossRef](#)]
- Liu, Y.X.; Li, W.Y.; Xu, J.C. The utilization of wavelet magnitude method of gravity anomaly in fault identification. *Geophys. Geochem. Explor.* **2014**, *38*, 96–99.
- Campbell, R.E. Multilevel aeromagnetic response curves over selected iron deposits and igneous rock types. *Lead. Edge* **2009**, *28*, 1198–1202. [[CrossRef](#)]
- Centeno, R.; Schou, J.; Hayashi, K. The helioseismic and magnetic imager (HMI) vector magnetic field pipeline: Optimization of the Spectral Line Inversion Code. *Sol. Phys.* **2014**, *289*, 3531–3547. [[CrossRef](#)]
- Duan, C.; Li, Y.H.; Wei, M.H. U-Pb dating study of detrital zircons from the Chuanlinggou Formation in Jiangjiazhai iron deposit, North China Craton and its geological significances. *Acta Petrol.* **2014**, *30*, 35–48.
- Osinowo, O.O.; Akanji, A.O.; Olayinka, A.I. Application of high resolution aeromagnetic data for basement topography mapping of Siluko and environs, southwestern Nigeria. *J. Afr. Earth Sci.* **2014**, *99*, 637–651. [[CrossRef](#)]
- Anderson, E.D.; Hitzman, M.W.; Monecke, T. Geological analysis of aeromagnetic data from southwestern Alaska: Implications for exploration in the area of the pebble porphyry Cu-Au-Mo deposit. *Econ. Geol.* **2013**, *108*, 421–436. [[CrossRef](#)]

22. Bansal, A.R.; Anand, S.P.; Rajaram, M. Depth to the bottom of magnetic sources (DBMS) from aeromagnetic data of central India using modified centroid method for fractal distribution of sources. *Tectonophysics* **2013**, *603*, 155–161. [[CrossRef](#)]
23. Ding, W.J.; Chen, Z.L.; Chen, B.L. Geochemical characters of band iron formations in Xingshan iron deposit in Qian'an area, Hebei Province: Implication for their origin. *J. Geomech.* **2009**, *15*, 363–373.
24. Mahdi, A.M.; Eldosouky, A.M.; Khateeb, S.O.E.; Youssef, A.M.; Saad, A.A. Integration of remote sensing and geophysical data for the extraction of hydrothermal alteration zones and lineaments; GabalShilman basement area, Southeastern Desert, Egypt. *J. Afr. Earth Sci.* **2022**, *194*, 104640. [[CrossRef](#)]
25. Bencharef, M.H.; Eldosouky, A.M.; Zamzam, S.; Boubaya, D. Polymetallic mineralization prospectivity modelling using multi-geospatial data in logistic regression: The Diapiric Zone, Northeastern Algeria. *Geocarto Int.* **2022**, *37*, 1–36. [[CrossRef](#)]
26. Ekwok, S.E.; Akpan, A.E.; Achadu, O.I.M.; Thompson, C.E.; Eldosouky, A.M.; Abdelrahman, K.; Andras, P. Towards Understanding the Source of Brine Mineralization in Southeast Nigeria: Evidence from High-Resolution Airborne Magnetic and Gravity Data. *Minerals* **2022**, *12*, 146. [[CrossRef](#)]
27. Eldosouky, A.M.; El-Qassas, R.A.Y.; Pham, L.T.; Abdelrahman, K.; Alhumimidi, M.S.; El Bahrawy, A.; Mickus, K.; Sehsah, H. Mapping Main Structures and Related Mineralization of the Arabian Shield (Saudi Arabia) Using Sharp Edge Detector of Transformed Gravity Data. *Minerals* **2022**, *12*, 71. [[CrossRef](#)]
28. Eldosouky, A.M.; El-Qassas, R.A.Y.; Pour, A.B.; Mohamed, H.; Sekandari, M. Integration of ASTER satellite imagery and 3D inversion of aeromagnetic data for deep mineral exploration. *Adv. Space Res.* **2021**, *68*, 3641–3662. [[CrossRef](#)]
29. Eldosouky, A.M.; Pham, L.T.; Henaish, A. High precision structural mapping using edge filters of potential field and remote sensing data: A case study from Wadi Umm Ghalqa area, South Eastern Desert, Egypt. *Egypt. J. Remote Sens. Space Sci.* **2022**, *25*, 501–513. [[CrossRef](#)]
30. Zhang, Y.D.; Song, J.S.; Gong, H.L. The relationship between distribution of iron deposits and characteristics of gravity and magnetic fields in Hebei Province. *Geophys. Geochem. Explor.* **2012**, *36*, 517–522.
31. Yang, Y.H.; Liu, S.; Hu, R.Z. Geochemistry and petrogenesis of the SanchakouMaifc Dyke in Chengde, Hebei Province, China. *J. Jilin Univ.* **2012**, *42*, 1796–1805.
32. Meng, G.X.; Yan, J.Y.; Lu, Q.T. Application of deep detecting technology in Hanxing subtype iron deposits and an integrated prospecting model: A case study of Baijian iron deposit. *Miner. Depos.* **2009**, *28*, 493–502.
33. Pan, L.H.; Li, L.Q.; Li, X. Sedimentary characteristics of the Jiufotang Formation developed in Luanping Mesozoic fault basin of northern Hebei Province. *J. Geomech.* **2010**, *16*, 85–95.
34. Shen, J.F.; Zhang, H.F.; Li, S.R. Timing and genesis of the Beiminghe iron deposit, south of the Taihang Mountain (TM). In Proceedings of the 34th International Geological Congress, Brisbane, Australia, 5–10 August 2012; p. 423.
35. Sun, J.; Du, W.H.; Wang, D.Z. Geological characteristics and genesis of the Heishan V-Ti magnetite deposit in Damiao, Chengde Hebei Province. *Acta Geol.* **2009**, *83*, 1344–1364.
36. Sun, H.Y.; Ma, X.; Niu, Y.J.; Gao, Y.L.; Liu, W. Application of high precision magnetic survey for exploration of iron and delineation of target areas in Longwangmiao iron deposit in Longhua county, Hebei province. *Geol. Surv. Res.* **2017**, *40*, 71–75.
37. Wang, Y.Q. Processing of magnetic anomaly data and application in the iron deposits in eastern Hebei Province. *Geol. Resour.* **2010**, *19*, 71–73.
38. Lu, Y.; Li, J.; Bai, X.S. Application of magnetic survey on hidden iron deposit prospecting: A case study on Luanping-II iron deposit in Hebei China. *J. Jilin Univ.* **2008**, *38*, 698–702.
39. Liu, D.B.; Shi, C.L.; Li, L.Y.; Zhao, Y.; Zhang, C.H. Geological characteristics and mining problems of Xuanlong iron ore deposit in Hebei province. *China Min. Mag.* **2016**, *25*, 94–97.
40. Li, W.Y.; Liu, Y.X.; Lu, W.F.; Ma, G.Q.; Zhang, C.S.; Zhao, J.W. Characteristics of Zhangsanying-Tongshanzi aeromagnetic anomaly zone and prospecting potential of iron deposits in northern Hebei, China. *Global Geol.* **2020**, *23*, 99–115.
41. Liu, Y.X.; Li, W.Y.; Yang, D.H.; Lu, W.F.; Wang, S.M. Study on characteristics of aeromagnetic anomaly and prospecting in Tuchengzi, Northwest Hebei Province. *Prog. Geophys.* **2019**, *34*, 2301–2308.
42. Liu, Y.X.; Li, W.Y.; Ma, G.Q.; Cao, A.Q.; Gao, S.; Wang, N.; Lu, W.F.; Wang, L.J.; Yang, C. Oil and gas basin analysis based on airborne gravity and magnetic data. *Appl. Geophys.* **2022**, *19*, 1–17. [[CrossRef](#)]
43. Zhang, Y.P.; Li, J.C. Tectonic framework and main characteristics of North China and its northward areas in Late Paleozoic-Early Mesozoic period. *Geol. China* **2010**, *37*, 916–930.
44. Zhang, L.C.; Zhai, M.G.; Zhang, X.J. Formation age and tectonic setting of the Shirengou Neoproterozoic banded iron deposit in eastern Hebei Province; constraints from geochemistry and SIMS zircon U/Pb dating Precambrian geology of China. *Precambrian Res.* **2012**, *222–223*, 325–338. [[CrossRef](#)]
45. Zhang, S.H.; Zhao, Y.; Liu, J.M. Geochronology, geochemistry and tectonic setting of the Late Paleozoic-Early Mesozoic magmatism in the northern margin of the North China Block: A preliminary review. *Acta Petrol. Mineral.* **2010**, *29*, 824–842.
46. Wang, B.D.; Wang, L.Q.; Chung, S.L.; Chen, J.L.; Yin, F.G.; Liu, H.; Li, X.B.; Chen, L.K. Evolution of the Bangong-Nujiang Tethyan ocean: Insights from the geochronology and geochemistry of mafic rocks within ophiolites. *Lithos* **2016**, *245*, 18–33. [[CrossRef](#)]
47. Wang, B.D.; Wang, L.Q.; Chen, J.L.; Liu, H.; Yin, F.G.; Li, X. Petrogenesis of Late Devonian-Early Carboniferous volcanic rocks in northern Tibet: New constraints on the Paleozoic tectonic evolution of the Tethyan Ocean. *Gondwana Res.* **2017**, *41*, 142–156. [[CrossRef](#)]
48. Zhai, M.G. Tectonic evolution and metallogenesis of North China Craton. *Miner. Depos.* **2010**, *29*, 24–36.

49. Xiang, P.; Cui, M.L.; Wu, H.Y. Geological characteristics, ages of host rocks and its geological significance of the Zhoutaizi iron deposit in Luanping, Hebei Province. *Acta Petrol.* **2012**, *28*, 3655–3669.
50. Zhao, Y.; Chen, B.; Zhang, S.H. Pre-Yanshanian geological events in the northern margin of the North China Craton and its adjacent areas. *Geol. China* **2010**, *37*, 900–915.
51. Li, W.Y.; Liu, Y.X.; Xu, J.C. Onshore Offshore Structure and Hydrocarbon Potential of the South Yellow Sea. *J. Asian Earth Sci.* **2014**, *90*, 127–136. [[CrossRef](#)]
52. Wang, B.D.; Chen, J.L.; Xu, J.F.; Wang, L.Q. Geochemical and Sr-Nd-Pb-Os isotopic compositions of Miocene ultrapotassic rocks in southern Tibet: Petrogenesis and implications for the regional tectonic history. *Lithos* **2014**, *208–209*, 237–250. [[CrossRef](#)]
53. Wang, B.D.; Wang, L.Q.; Chen, J.L.; Yin, F.G.; Wang, D.B.; Zhang, W.P.; Chen, L.; Liu, H. Triassic three-stage collision in the Paleo-Tethys: Constraints from magmatism in the Jiangda–Deqen–Weixi continental margin arc, SW China. *Gondwana Res.* **2014**, *26*, 475–491. [[CrossRef](#)]